

LEVEL



DNA 5686F

A COMPUTER MODEL FOR HIGH-LATITUDE PHASE SCINTILLATION BASED ON WIDEBAND SATELLITE DATA FROM POKER FLAT

AD A105620

Edward J. Fremouw
John M. Lansinger
Physical Dynamics, Inc.
P.O. Box 3027
Bellevue, Washington 98009

28 February 1981

Final Report for Period 15 August 1979—28 February 1981

CONTRACT No. DNA 001-79-C-0372

APPROVED FOR PUBLIC RELEASE;
DISTRIBUTION UNLIMITED.

THIS WORK SPONSORED BY THE DEFENSE NUCLEAR AGENCY
UNDER RDT&E RMSS CODE B322079464 S99QAXHB05421 H2590D.

Prepared for
Director
DEFENSE NUCLEAR AGENCY
Washington, D. C. 20305

DTIC
ELECTE
S OCT 16 1981 **D**

D

01 10 16

DTIC FILE COPY

xi

Destroy this report when it is no longer
needed. Do not return to sender.

PLEASE NOTIFY THE DEFENSE NUCLEAR AGENCY,
ATTN: STTI, WASHINGTON, D.C. 20305, IF
YOUR ADDRESS IS INCORRECT, IF YOU WISH TO
BE DELETED FROM THE DISTRIBUTION LIST, OR
IF THE ADDRESSEE IS NO LONGER EMPLOYED BY
YOUR ORGANIZATION.



UNCLASSIFIED

SECURITY CLASSIFICATION OF THIS PAGE (When Data Entered)

REPORT DOCUMENTATION PAGE		READ INSTRUCTIONS BEFORE COMPLETING FORM	
1. REPORT NUMBER DNA 5686F	2. GOVT ACCESSION NO. AD-A105620	3. RECIPIENT'S CATALOG NUMBER	
4. TITLE (and Subtitle) A COMPUTER MODEL FOR HIGH-LATITUDE PHASE SCINTILLATION BASED ON WIDEBAND SATELLITE DATA FROM POKER FLAT		5. DATE OF REPORT & PERIOD COVERED Final Report for Period 15 Aug 79 - 28 Feb 81	
7. AUTHOR(s) Edward J. Fremouw and John M. Lansinger		6. PERFORMING ORG. REPORT NUMBER PD-NW-81-240R	
9. PERFORMING ORGANIZATION NAME AND ADDRESS Physical Dynamics, Inc. P. O. Box 3027 Bellevue, Washington 98009		8. CONTRACT OR GRANT NUMBER(s) DNA 001-79-C-0372	
11. CONTROLLING OFFICE NAME AND ADDRESS Director Defense Nuclear Agency Washington, D.C. 20305		10. PROGRAM ELEMENT, PROJECT, TASK AREA & WORK UNIT NUMBERS Subtask S99QAXHB054-21	
14. MONITORING AGENCY NAME & ADDRESS (if different from Controlling Office)		12. REPORT DATE 28 February 1981	
		13. NUMBER OF PAGES 54	
		15. SECURITY CLASS. (of this report) UNCLASSIFIED	
		15a. DECLASSIFICATION/DOWNGRADING SCHEDULE N/A	
16. DISTRIBUTION STATEMENT (of this Report) Approved for public release; distribution unlimited.			
17. DISTRIBUTION STATEMENT (of the abstract entered on block 20, if different from Report)			
18. SUPPLEMENTARY NOTES This work is sponsored by the Defense Nuclear Agency under RDT&F RMSS Code 0322079464 S99QAXHB05421 H2590D.			
19. KEY WORDS (Continue on reverse side if necessary and identify by block number) Radiowave scintillation, Phase scintillation, Auroral scintillation, Ionospheric irregularities, Plasma striation, Scintillation model, Computer model			
20. ABSTRACT (Continue on reverse side if necessary and identify by block number) A mathematical model has been developed for describing plasma-density irregularities responsible for radiowave scintillation produced in the auroral ionosphere, and the model has been committed to an applications-oriented computer code, WMOD. The model characterizes the three-dimensional configuration, gradient sharpness, and height-integrated strength of irregularities represented by a power-law spatial spectrum as functions of geomagnetic latitude, time of day, sunspot number, and planetary geomagnetic activity			

DD FORM 1 JAN 73 1473

UNCLASSIFIED

SECURITY CLASSIFICATION OF THIS PAGE (When Data Entered)

393400

JOB

UNCLASSIFIED

SECURITY CLASSIFICATION OF THIS PAGE (When Data Entered)

20. ABSTRACT (Continued)

index. Program WBMOD permits calculation of the power-law index and spectral strength (at a fluctuation frequency of 1 Hz) of phase scintillation, together with scintillation indices (variances) for phase and intensity, using a phase-screen scattering theory.

The model has been calibrated and iteratively tested against phase-scintillation data from the DNA Wideband Satellite Experiment, collected at Poker Flat, Alaska. It does not account for seasonal variations in high-latitude scintillation observed in other longitude sectors. The program contains a model for middle-latitude and equatorial irregularities as well as for auroral latitudes, but only the latter has been tested extensively against high-quality scintillation data.

UNCLASSIFIED

SECURITY CLASSIFICATION OF THIS PAGE (When Data Entered)

TABLE OF CONTENTS

<u>Section</u>	<u>Page</u>
LIST OF ILLUSTRATIONS -----	2
LIST OF TABLES -----	4
I. INTRODUCTION -----	5
II. OVERVIEW OF WBMOD -----	6
A. STRUCTURE OF THE CODE -----	6
B. THE SCINTILLATION CALCULATIONS -----	8
III. THE MODEL -----	18
A. OVERVIEW -----	18
B. THREE-DIMENSIONAL CONFIGURATION -----	21
C. HEIGHT-INTEGRATED IRREGULARITY STRENGTH -----	28
IV. USE OF THE CODE -----	40
V. CONCLUSION -----	44
REFERENCES -----	46

Accession For	
NTIS GRA&I	<input checked="" type="checkbox"/>
DTIC TAB	<input type="checkbox"/>
Unannounced	<input type="checkbox"/>
Justification	
By _____	
Distribution/	
Availability Codes	
Dist	Avail and/or Special
A	1

S DTIC ELECTE **D**
 OCT 16 1981
D

LIST OF ILLUSTRATIONS

<u>Figure</u>		<u>Page</u>
1	Flow diagram for Program WBMOD -----	7
2	Relationship between VHF phase spectral index, p , and geomagnetic L value at the line-of-sight penetration point in the F layer. (After Fremouw and Lansinger, 1979.) -----	20
3	Observed distribution of phase-scintillation index, σ_ϕ , with angle between the line of sight and the local magnetic L shell for 58 nighttime passes nearly along the magnetic meridian. -----	23
4	Relationship between field-line-axial ratio, a , and width of geometrical scintillation enhancement for nearly overhead passes, showing observed width and deduced value of a . -----	24
5	Relationship between L-shell axial ratio, b , and width of geometrical scintillation enhancement for nighttime passes to the east and west of Poker Flat, showing observed widths and accepted value of b . Horizontal uncertainty bars on $b = 6$ point indicate spread calculated for range of geometries included in data sets employed. -----	26
6	Sunspot-number dependence of nighttime, VHF phase-scintillation index at Poker Flat. Ordinate values represent monthly means. -----	30
7	Comparisons of nighttime, VHF phase scintillation index calculated (solid) by means of Program WBMOD and observed (broken) at Poker Flat, Alaska in the Wideband Satellite Experiment. Left: pre-midnight passes to the east of the station. Center: near-midnight passes essentially along the geomagnetic meridian. Right: post-midnight passes to the west of the station. Bottom: $0 \leq K_p \leq 2+$. Top: $3- \leq K_p \leq 5+$. No. of passes in each data set is indicated in the upper righthand corner of each grid. Calculated values are for a single representative pass. -----	36

LIST OF ILLUSTRATIONS (continued)

<u>Figure</u>		<u>Page</u>
8	Comparison of WBMOD (solid) results and observed values (broken) of daytime VHF phase scintillation index. Left-overhead (morning) passes. Right: west (late morning) passes. Bottom: $0 \leq K_p \leq 2+$. Top: $3- \leq K_p \leq 5+$. No. of passes as indicated in the upper righthand corner of each grid. -----	38
9	Comparison of model results (solid) and observed values (broken) of VHF phase scintillation index for geomagnetically very disturbed ($K_p \geq 6-$) nighttime (left) and daytime (right) conditions. -----	39
10	Comparison of model results (solid) with observed values (broken) of VHF phase scintillation index from two dissimilar data sets not used in iterative development of the model. -----	45

LIST OF TABLES

<u>Table</u>		<u>Page</u>
1	Subroutines and Functions in Program WEMOD -----	9
2	Sample Input Interaction Between WEMOD and User -----	41
3	Sample WEMOD Output -----	42

I. INTRODUCTION

A variety of modern military systems used for communication, navigation, and surveillance depends upon transmission of radio signals through the ionosphere. Thus, description and understanding of ionospheric structure in scale-size regimes that can distort trans-ionospheric radio waves are research topics of interest to several elements of the Department of Defense. Moreover, high-altitude nuclear plasmas become structured under the influence of various instabilities, and the resulting striations scatter radio waves to produce phase and intensity scintillations.

As a result of the common physics underlying the scintillation phenomenon arising in both the naturally disturbed and nuclear-perturbed ionosphere, the Defense Nuclear Agency (DNA) and its community of contractors have developed considerable expertise in describing the plasma structures, resulting scintillations, and pursuant effects on radars and communication systems. Among the techniques used by the DNA community in studying scintillation effects has been propagation of radio signals through structures that develop in non-nuclear plasmas, including transmission of carefully designed signals from the DNA Wideband satellite through the naturally striated ionosphere (Fremouw et al, 1974; Rino et al, 1977; Fremouw et al, 1978).

Signal-statistical aspects of the Wideband results (Fremouw and Miller, 1978) have been applied to systems evaluations (Scott and Knepp, 1978), and the experiment has provided guidance to propagation theorists tailoring their work to the solution of relevant engineering problems (Rino and Matthews, 1978). In response to a specific system need, DNA contracted Physical Dynamics to summarize a portion of the Wideband data base by committing it to an applications-oriented computer model. The task set forth was to develop a model, based on Wideband data from Poker Flat, Alaska (64.8° invariant; 65.1° N, 147.5° W), to be used for engineering evaluation of effects to be expected from auroral-zone scintillation. This document is the final report on the contract let to accomplish that task.

The model code, WBMOD, is based on earlier work by Fremouw and Bates (1971), Fremouw and Rino (1973), and Fremouw et al (1977a). The code's structure and the phase-screen scattering theory (Rino, 1979a) underlying its scintillation calculations are briefly described in Section II. The irregularity model that forms the heart of WBMOD is presented in Section III. Simple running instructions are given in Section IV, and the report is concluded in Section V, which includes caveats about applications and plans for further improvement of the model.

II. OVERVIEW OF WBMOD

A. STRUCTURE OF THE CODE

The predecessor of Program WBMOD was Program IONSCNT, which was described in detail by Rino et al (1978). There are two major differences between WBMOD and IONSCNT. First, the new code is much simpler. Second, WBMOD contains the best available mathematical descriptions of the shape and strength of scintillation-producing irregularities in the auroral zone, contained respectively in Subroutine MDLPRM and Function CSL. The bulk of the work under this contract was directed at development of those descriptions by means of iterative modeling against Wideband Satellite data from Poker Flat.

Figure 1 is a flow diagram of Program WBMOD. Upon initiation of the program, the user is asked for information regarding his computational scenario. The requested information includes parameters of the user's system, such as operating frequency and the reciprocal of a high-pass cutoff for phase fluctuations (i.e., the longest time over which the system's mission requires phase stability). It also includes other aspects of the intended operation, such as transmitter and receiver location and time of day, plus characterization of the general state of solar-terrestrial disturbance by means of sunspot number and planetary magnetic activity index, K_p . Finally, the user specifies one of his input quantities as the independent variable (e.g., transmitter location or time of day). Various indicators of scintillation strength (i.e., scintillation indices), which are described fully in Section IIB, are calculated as functions of the selected independent variable.

Control of WBMOD computations is quickly relinquished by the driver program to three major subroutines, READIN, SCINT1, and SCINT3. In addition to calling for program inputs, READIN controls many of the computations that are peripheral to calculation of the scintillation indices themselves. Since scintillation severity is highly geometry-dependent, much of the code is involved in geometrical computations, and some of these are controlled by READIN.

Among the parameters that the user may choose to vary are the receiver or transmitter latitude/longitude coordinates (RCRD and TCRD respectively). This may be done either in an incremental but static manner or in an orbital mode (ORBT), in which the scanning motion of the line of sight is taken into account. (In all modes but ORBT, scintillation is taken to arise solely from drift of ionospheric irregularities across a stationary line of sight.)

If one of the moving-terminal modes (RCRD, TCRD, or ORBT) is chosen, the first calculation determines the azimuth and great-circle angle between the start and end points; this computation is performed in Subroutine AZNGCA. In the two CRD modes, the terminal position

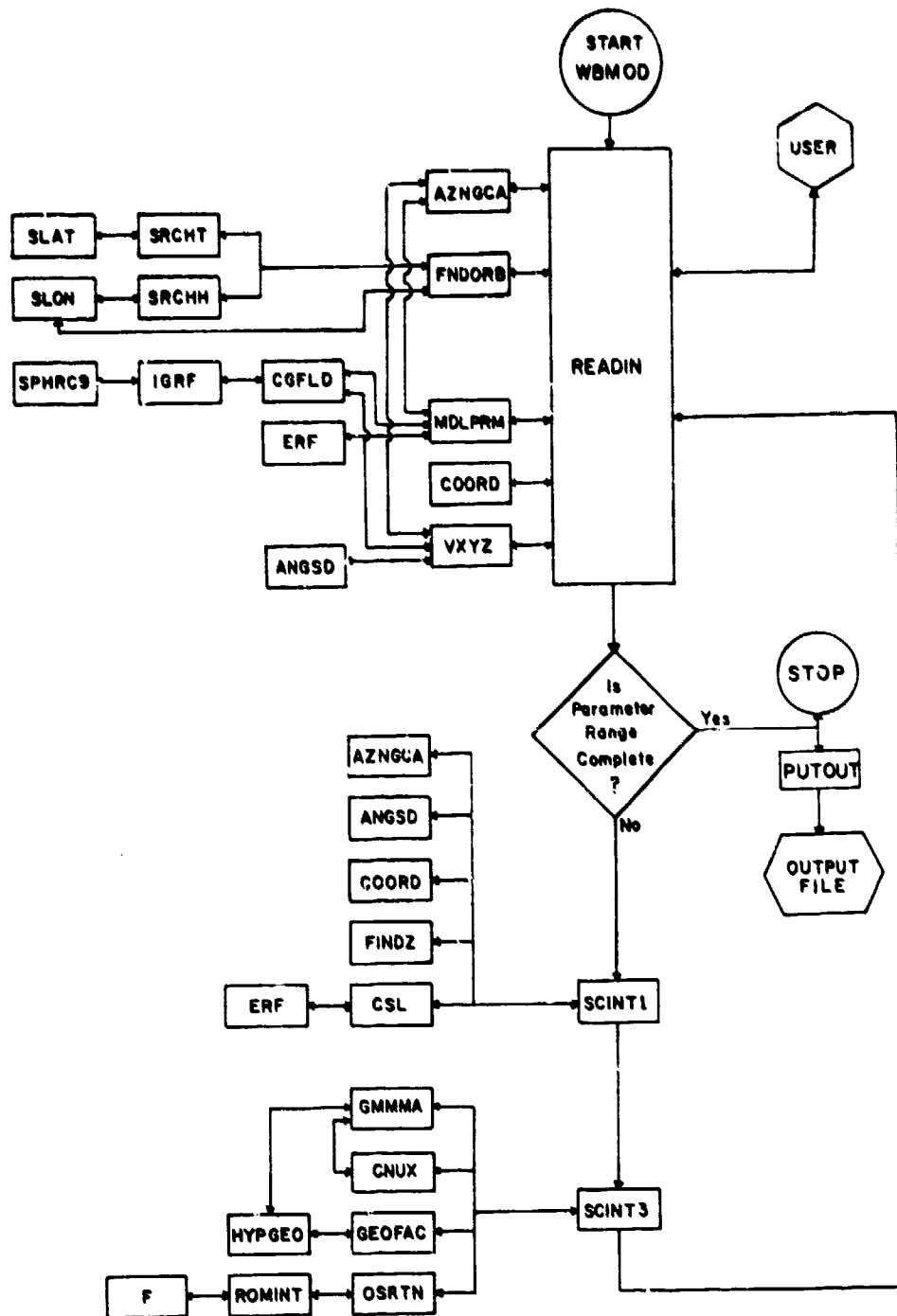


Figure 1. Flow diagram for Program WBMOD.

is incremented by the number of steps specified by the user. In the ORBT mode, it is moved in equal increments of time along a circular orbit at a user-specified altitude, by means of Subroutine FINDORB and its subordinates, Functions SLAT and SLON and Subroutines SRCHT and SRCHH.

Whether the variable parameter is a terminal location or some other independent variable (e.g., K_p or sunspot number), its incrementing is controlled by READIN. The first implementation of the irregularity model is made by means of calls to MDLPRM, which calculates all parameters describing the irregularities except their strength. Simple models for irregularity drift velocity and height of the scattering layer, upon which the line-of-sight scan velocity depends, are invoked at this time to complete certain geometry calculations.

If the user has not specified an irregularity drift velocity (i.e., if he has defaulted by entering "model" when asked), the code will employ the rudimentary drift model contained in MDLPRM. If the user has selected the ORBT mode, the drift velocity is added to the scan velocity calculated in Subroutine VXYZ and its subordinates. The scan velocity dominates over the drift velocity in typical low-orbiting scenarios, in which case the drift is not very important.

While the geometry is calculated in geodetic coordinates, all of its aspects that control radiowave scatter and the development of scintillation must account for orientation of the geomagnetic field. Thus, MDLPRM and VXYZ rely upon Subroutine CGFLD, which sets up calls to the International Geomagnetic Reference Field (Trombka and Cain, 1974) contained in Subroutine IGRF and its subordinate, Subroutine SPHRC9. In addition, READIN calls Subroutine COORD, which locates incremented points along a great circle, and VXYZ employs plane-geometry information from Subroutine ANGSD.

As READIN increments the calculations, it also checks for completion of the number of increments specified by the user, whereupon it calls on Subroutine PUTOUT to list the computation results in an output file. Until completion is accomplished, READIN passes control back to the driver during each increment cycle, and the driver calls Subroutines SCINT1 and SCINT3 in sequence to carry out the main scintillation computations. Table 1 contains synoptic descriptions of all WBMOD subroutines and functions.

B. THE SCINTILLATION CALCULATIONS

Subroutine SCINT1 plays a preparatory roll for calculating the scintillation parameters. Its two main functions are (1) to establish the scattering geometry at the ionospheric penetration point of the line of sight and (2) to provide the strength of scintillation-producing irregularities at that point, calculated from the model as Function CSL.

Table 1
Subroutines and Functions in Program WBMOD

Name	Synopsis
WBMOD	Driver Routine.
READIN	Calls for inputs from user and certain subroutines, and increments changing parameter(s).
AZNGCA	Finds azimuth and great-circle angle between points 1 and 2, using double precision.
FINDORB	Finds circular orbit between two points at a given altitude.
SRCHT	Finds orbital phase.
SLAT	Computes satellite latitude.
SRCHH	Finds hour angle of orbital plane.
SLON	Computes satellite longitude.
MDLPRM	Establishes all parameters of the ionospheric irregularity model except height-integrated strength.
ERF	Computes error function in double precision.
CGFLD	Sets up calls to spherical harmonic model of geomagnetic field.
IGRF	Contains International Geomagnetic Reference Field model and returns x, y, z components of field.
SPHRC9	Operates in conjunction with IGRF.
COORD	Finds point 2 given point 1 and azimuth and great-circle angle between them, using double precision.
VXYZ	Calculates line-of-sight scan velocity, using double precision.
ANGSD	Plane-geometry routine.
SCINT1	Establishes scattering geometry at ionospheric penetration point and calls up information on strength of irregularities.
FINDZ	Calculates "reduced height" for one-way and two-way propagation.
CSL	Computes height-integrated strength of irregularities from empirical model.
SCINT3	Calculates scintillation parameters using phase-screen scattering theory.
GMMA	Gamma-function routine.
CNUX	Calculates normalization factor used in computation of intensity scintillation index.
GEOFAC	Calculates static and dynamic geometrical factors that influence scintillation strength.

Table 1 (continued)
Subroutines and Functions in Program WBMOD

<u>Name</u>	<u>Synopsis</u>
HYPGEO	Calculates Gaussian hypergeometric function.
OSRTN	Sets up integral to calculate phase variance, for finite outer scale.
ROMINT	Modified Romberg quadrature integration routine.
F	Computes change of variable for efficient integration by ROMINT.
PUTOUT	Formats and controls output.

ACOS	Computes \cos^{-1} in double precision
ASIN	Computes \sin^{-1} in double precision.
TAN	Computes tan.

For its first task, SCINT1 calls upon several subroutines used earlier. Subroutines used by VXYZ and READIN to deal with the changing geometry called for by the ORBT mode are now used to calculate the instantaneous scattering geometry for any mode. For instance, AZNGCA now returns the azimuth and great-circle angle between the transmitter and receiver (or a radar and reflection point), and COORD calculates the latitude and longitude of the penetration point lying in that great-circle sector. The geomagnetic invariant latitude, calculated in MDLPRM after its call to CGFLD, is passed to SCINT1 from READIN through their respective call arguments. As its final geometrical contribution, SCINT1 calls FINDZ to calculate a "reduced-height" parameter needed for establishing the size of the Fresnel zone. The Fresnel-zone size, which is different for one-way and two-way propagation, is employed for calculating the intensity scintillation index.

For its second task, SCINT1 makes the code's only request for information on irregularity strength by invoking Function CSL. The other key information about the irregularities, which describes their three-dimensional configuration and height, has already been calculated by Subroutine MDLPRM and passed directly to SCINT3 in Common Block OMP. The contents of MDLPRM and CSL will be described in detail in Sections III B and C, respectively.

The direct scintillation calculations are made in Subroutine SCINT3, which makes use of the phase-screen scattering theory of Rino (1979a). The central quantity calculated is T, which in Rino's original infinite outer-scale formulation numerically equals the power spectral density of phase at a fluctuation frequency of 1 Hz. It is given by

$$T = \lambda^2 r_e^2 \frac{\sqrt{\pi} \Gamma(\nu)}{(2\pi)^{2\nu+1} \Gamma(\nu+\frac{1}{2})} C_s L(\sec \theta) G v_e^{2\nu-1}, \quad (1)$$

where λ = radio wavelength,
 r_e = classical electron radius,
 θ = incidence angle of the propagation vector on the (horizontal) scattering layer.

The gamma functions arise from normalizing the three-dimensional ionospheric spectrum to the electron-density variance, $\langle (\Delta N)^2 \rangle$, such that

$$C_s = 8\pi^{3/2} \frac{\Gamma(\nu + \frac{1}{2})}{\Gamma(\nu - 1)} \frac{\langle (\Delta N)^2 \rangle}{\alpha^{(2\nu-2)}}, \quad (2)$$

which is (to within a factor α^* , which Rino chose to incorporate in the geometrical factor, G) numerically equal to the strength of the three-dimensional spectrum at a (nonisotropic)

*Defined on p. 12.

wave number of 1 rad/m. The spectrum itself is taken to be of the form $C_g \kappa^{-\eta}$ in the spectral regime responsible for scintillation, but to be held finite by an outer scale, α .

The gamma-function arguments depend only upon the sharpness of electron-density gradients, expressed as a spectral parameter given by

$$\nu = \frac{\eta - 1}{2} . \quad (3)$$

The corresponding one-dimensional (*in-situ*) spectral index is $2\nu-1$ (Cronyn, 1970), and the two-dimensional (phase) spectral index is

$$p = 2\nu . \quad (4)$$

The height-integrated spectral strength of the irregularities, $C_g L$, is the quantity obtained from Function CSL, and our model for it will be described in detail in Section III C. Conceptually, C_g is a structure constant characterizing the irregularity strength, and L is the (vertical) thickness of the irregular layer, but it is their product that is modelled from Wideband data.

The two remaining quantities in Eq. (1), G and V_e , describe respectively the static and dynamic aspects of geometrical control over phase scintillation. They are calculated in Subroutine GEOFAC, which is called by SCINT3, as follows:

$$G = \frac{a b}{\sqrt{AC - B^2/4} \cos\theta} \quad (5)$$

and

$$V_e = \frac{(CV_{sx}^2 - BV_{sx}V_{sy} + AV_{sy}^2)^{1/2}}{\sqrt{AC - B^2/4}} , \quad (6)$$

where a = field-aligned axial ratio (ratio of irregularity size along the geomagnetic field to that normal to the field in a reference direction.),

b = second axial ratio for describing sheetlike irregularities (ratio of irregularity size in direction normal to both the geomagnetic field and the reference direction to that in the reference direction);

and \vec{V}_s = a foreshortened horizontal projection of the line-of-sight scan velocity calculated in Subroutine VXYZ and defined in Eq. (14) of Rino (1979a).

3

The geometrical factors, A, B, and C, which are defined in Eq. (41) of Rino and Fremouw (1977), depend upon the incidence angle, θ , and magnetic heading, ϕ , of the propagation vector in addition to a and b. They depend also on the geomagnetic dip angle, ψ , and on a final irregularity parameter, δ , which is the angle that sets the reference direction for defining b.

The physical fact accounted for by the static geometrical enhancement factor, G, is that the phase perturbation imposed on a radio wave propagating along an extended dimension of irregularities builds up quasi-coherently, as compared with that for propagation along a short dimension. The description of this fact depends upon the propagation direction defined by θ and ϕ , the anisotropy of the irregularities defined by a and b, and the orientation of the irregularities defined by ψ and δ .

The physical fact described by the effective velocity, V_e , is that a low-pass spatial spectrum results in stronger spectral density at a given temporal frequency (1 Hz) not only for greater scan velocities, but also for scans across short irregularity dimensions as compared with long ones. Thus, V_e depends not only on V_s but also on θ , ϕ , ψ and a, b, δ . A high-inclination satellite observed from a high-latitude station typically moves rapidly across field-aligned-irregularity contours for the same look angles at which its line of sight is nearly parallel to the field. In this situation, the contributions of G and V_e to enhancement of phase scintillation near the geomagnetic zenith reinforce one another, and geometric enhancement is very strong. This combination of effects extends to a geomagnetic east-west line across the sky for irregularities extended along L shells (Fremouw et al, 1977b; Rino, Livingston, and Matthews, 1978).

The fundamental outputs from WEMOD are T and p, which respectively are measures of the strength and spectral character of phase scintillation. The power-law spectral index, p, of phase is obtained from Eq. (4), which ignores the effect of diffraction on the shape of the phase spectrum. Diffractive alteration of p is believed to occur, but to be quite subtle (Livingston et al, 1981), and the state of scintillation theory does not permit its calculation in general. Moreover, as we shall see in Section III B, we have modelled ν (and, therefore, p) as a constant because it is much less variable than other parameters such as irregularity strength, $C_s L$, and because little is known about its variability. The code is structured so that future research results about spectral index could be incorporated in Subroutine MDLPRM. At present, WEMOD employs a value of 1.25 for ν and outputs the corresponding value of p (2.50).

Unlike p , the strength, T , of phase scintillation is highly variable. The large majority of WBMOD is given over to calculating T and two commonly used indices of scintillation activity based on it, one for phase and one for intensity. The scintillation index for phase is simply its standard deviation, σ_ϕ , which may be calculated by integrating the phase-scintillation temporal spectrum, $\phi_\phi(f)$, as follows:

$$\sigma_\phi^2 = \int_{f_c}^{\infty} \phi_\phi(f) df = \int_{f_c}^{\infty} \frac{T df}{(f_o^2 + f^2)^{p/2}}, \quad (7)$$

where

$$f_o = v_e / 2\pi\alpha. \quad (8)$$

(The outer scale, α , is measured in rad/m in the field-normal reference direction used in defining a and b , at the $2^{(v-1/2)}$ -point on the in-situ power spectrum.)

In Eq. (7), f_c is the lowest phase-fluctuation frequency to which the system is sensitive. For instance, in the Wideband satellite experiment with normal processing, f_c was 0.1 Hz (Fremouw et al, 1978) as set by phase detrending. In a coherently integrating radar, it would be the reciprocal of the time over which phase coherence is required. For systems not sensitive to phase instability in the propagation medium, f_c is effectively infinite, and the effective σ_ϕ is zero.

Equation (7) may be evaluated for three ranges of the ratio f_c/f_o , as follows:

$$\sigma_\phi^2 \left\{ \begin{array}{l} \approx \frac{2Tf_c(1-p)}{(p-1)} \quad ; \quad \frac{f_c}{f_o} \gg 1 \quad (9a) \\ = T f_o^{(1-p)} \left\{ \pi \frac{\Gamma(\frac{p}{2} - \frac{1}{4})}{\Gamma(\frac{p}{2})} - 2 \left(\frac{f_c}{f_o}\right) {}_2F_1 \left[\nu, \frac{1}{2}; \frac{3}{2}; -\left(\frac{f_c}{f_o}\right)^2 \right] \right\} ; \quad \frac{f_c}{f_o} \lesssim 1 \quad (9b) \\ \approx \pi \frac{\Gamma(\frac{p}{2} - \frac{1}{4})}{\Gamma(\frac{p}{2})} T f_o^{(1-p)} \quad ; \quad \frac{f_c}{f_o} \ll 1 \quad (9c) \end{array} \right.$$

where ${}_2F_1$ is the Gaussian hypergeometric function. Unfortunately, an analytical evaluation of Eq. (7) has not been found in the range $f_c/f_o \gtrsim 1$.

The ionospheric outer scale, α , is sufficiently large that Eq. (9a) is quite valid over the range of effective velocity, V_e , encountered in the Wideband experiment, and we have employed it for much of our modeling. Moreover, the magnitude and variational behavior of α are not known. While the outer scale appears to be quite large compared with the spatial windows of a number of ionospheric experiments, there is no assurance that Eq. (9a) is valid for all systems in all operating scenarios. Accordingly, SCINT3 contains an efficient means (Subroutine OSRTN and Function F) for numerically evaluating Eq. (7), so that the code is not restricted inherently to application in the infinite outer-scale limit.

We have established that Eq. (9a) overestimates σ_ϕ by no more than 0.1% for $f_c/f_o \geq 20$. The f_c/f_o ratio is calculated in SCINT3, and σ_ϕ is calculated directly from Eq. (9a) for ratio values greater than 20. For values of 20 or smaller, SCINT3 calls Subroutine OSRTN for numerical evaluation of Eq. (7). At present, α is set at a very large constant value (10^6 m), so Eq. (9a) is employed in any likely application. An option is provided for the user to override this default value should he want to investigate the effect of varying the outer scale. The main reason for coding Eq. (7), however, is to prepare for ready inclusion of any new results on the ionospheric outer scale that may be yielded by research programs.

The scintillation index for intensity is the ratio, S_4 , of the standard deviation of received signal power to the mean received power (Briggs and Parkin, 1963). Unlike σ_ϕ , its relation to T is set not by a system or ionospheric parameter, but by the diffraction process that gives rise to intensity scintillation. For weak to moderate levels of intensity scintillation, S_4^2 is very well approximated (Rino, 1979a and Fremouw, 1980a) by

$$S_{4w}^2 = C(v) \frac{T}{V_e} \frac{F}{(2v-1)G} Z^{v-1/2} \quad (10)$$

where

$$C(v) \left\{ \begin{array}{l} = \frac{2^{3v-1/2} \pi^{2v+1/2} \cos \pi \left(\frac{v}{2} - \frac{1}{4} \right)}{-\Gamma(v) \cos \pi v} ; v \neq 1.5 \\ = 16 \pi^3 ; v = 1.5 \end{array} \right. \quad (11a)$$

$$F = \frac{a b}{\sqrt{A''} C'' v} {}_2F_1 \left(\frac{1}{2} - v, \frac{1}{2}; 1; \frac{A'' - C''}{A''} \right) \quad (12)$$

$$\text{and } Z = \frac{\lambda z \sec \theta}{4\pi} \quad (13)$$

In the foregoing, A'' and C'' are geometrical parameters derived from A , B , and C by means of a coordinate rotation (Rino, 1979a), and z is the effective "reduced height" (including correction for wave-front curvature and curved-earth geometry) of the irregularities.

The two geometrical enhancement factors, G and V_e , that appear in Eq. (1) divide out of Eq. (10). The Fresnel filter factor, F , behaves in a fashion similar to G , however, and intensity scintillation also undergoes a geometrical enhancement. Nonetheless, it is a weaker enhancement than that experienced in phase scintillation, due to the difference in V_e -dependence. In addition to describing static geometrical enhancement, F accounts for the effect of diffraction, together with the Fresnel-zone parameter, Z .

Now, Eq. (10) is a weak-scintillation formula. For practical purposes, however, it may be generalized to include the well-known saturation of S_4 at unity by writing

$$S_4^2 = 1 - \exp(-S_{4w}^2) . \quad (14)$$

Equation (14) is exact for scintillating signals that obey Rice statistics (Fremouw and Rino, 1976). Use of it ignores some effects of geometrical-optics focusing, which can drive S_4 modestly above unity (to 1.3 in rare and isolated instances) and which subtly alter the signal statistics accompanying scintillation (Fremouw, Livingston, and Miller, 1980). While considerable progress has been made in recent years on multiple-scatter theory (Rumsey, 1975; Rino, 1979b), a fully general expression for S_4 (the saturation behavior of which would depend upon ν) is not yet available. Comparison of the behavior of S_4 and σ_ϕ , as measured in the Wideband experiment, shows that Eq. (14) is quite adequate to represent the behavior of S_4 for presently identified applications of WBMOD, and it has been coded into SCINT3.

The scintillation theory sketched in the foregoing discussion is well worked out for one-way propagation. For phase scintillation, the adaptation to two-way propagation is trivial. The round-trip propagation time is short compared with all other relevant time scales. Thus, the radio wave encounters the same irregularities twice, which doubles the phase perturbation and therefore quadruples its variance, σ_ϕ^2 , and power-spectral density, T . Accordingly, when a user chooses two-way propagation, WBMOD multiplies Eq. (1) by 4 to obtain the value of T that is output and used in Eqs. (7, 9a, and 10).

Single-scatter considerations lead to a simple adaptation of Eq. (10) for describing intensity scintillation in two-way propagation. The effective reduced range is calculated for a scattering geometry that accounts for an image source and scattering region (the ionosphere encountered on the downlink), as well as for scattering on the uplink. A full

accounting for multiple-scatter effects in two-way propagation probably would be difficult to attain in terms of simple phase-screen theory. These effects, however, probably would be seen primarily in the time structure of intensity scintillation and in relative subtleties of signal statistics, rather than having a significant influence on S_4 . We employ Eq. (14) as a multiple-scatter correction for two-way as well as for one-way propagation.

III. THE MODEL

A. OVERVIEW

In order to calculate T , p , σ_{ϕ} , and S_4 , one must have values for eight parameters describing ionospheric irregularities. They are: the height, h , and vector drift velocity, \vec{v}_d , of the irregularities; an outer scale, α ; four "shape" parameters describing the irregularities' three-dimensional configuration and spatial "sharpness", a , b , δ , and ν ; and the height-integrated spectral strength, $C_g L$. In principle, one needs descriptive models for all eight of these parameters. Fortunately, the degree of descriptive detail needed for the parameters is quite different for the different parameters, depending somewhat upon the application of results.

Program WBMOD contains models for the above eight parameters, but the degree of detail is very much less for some than for others. As alluded to in Section II B, the "model" for outer scale is a single, effectively infinite (10^6 m), constant value. An effectively infinite value is the most realistic approach to providing useful outputs for known types of users, given the current state of ionospheric knowledge, and subject to simple modification for special studies if desired.

The "model" for drift velocity is almost equally rudimentary. In m/sec, it is as follows:

$$v_{dx} = 0 \quad (15a)$$

$$v_{dy} = 50 - 15 \left(1 + \operatorname{erf} \frac{\lambda_m - 20^\circ}{3^\circ} \right) + 40(1 + K_p) \left(1 + \operatorname{erf} \frac{\lambda_m - \lambda_b}{3^\circ} \right) \quad (15b)$$

$$v_{dz} = 0 \quad (15c)$$

where erf = error function,

λ_m = geomagnetic invariant latitude,

and where x , y , and z denote components respectively in the geomagnetic north and east and the downward directions. Equation (15) describes an eastward drift of 50 m/sec at the geomagnetic equator, dropping to 20 m/sec at middle latitudes, and increasing with geomagnetic disturbance at latitudes above that, λ_b , of the high-latitude scintillation boundary. This description is in need of review, especially at high latitudes. It has not been revised under the present contract because it is of little importance for the main identified application. Users with phase-sensitive applications involving geostationary satel-

lites are advised to make use of the option provided for external specification of values for \vec{V}_d . (Drift velocity is of no consequence for WBMOD application to systems susceptible only to intensity scintillation, and of little importance in even phase-sensitive low-orbit applications.)

A rudimentary description of the effective (centroid) height, h , of scintillation-producing irregularities in the F layer also is included in WBMOD, as follows:

$$h = 500 - 75(1 + \operatorname{erf} \frac{\lambda_m - 20^\circ}{3^\circ}) \text{ km} . \quad (16)$$

That is, the equivalent phase-changing screen is taken to be at about the middle of the F layer, 350 km, except near the geomagnetic equator where nighttime scintillation seems to arise in a layer extended to considerable height. During this work, some investigation was made of the effect of layer height on phase scintillation, specifically by lowering it in the auroral oval. A lower height clearly decreases T and α_ϕ because the slower scan through the irregular layer decreases the effective velocity. (See Eq. 6.) No sound basis was found, however, for changing layer height by means of comparison with phase-scintillation data, which was the main thrust of the present work. A worthwhile improvement in Eq. (16) might be possible on the basis of observed values of S_4/σ_ϕ .

With the relatively unimportant (for present purposes) and currently uncertain parameters (α , \vec{V}_d , and H) accounted for, we now consider the more systematic aspects of the modeling procedure. Prior to the Wideband experiment, *in-situ* measurements of ionospheric irregularities were generally reported as indicating a one-dimensional power-spectral index of about 2, which would translate to a phase spectral index, p , of 3 and a value of 1.5 for ν . Our approach to scintillation modeling was predicated on being able to treat ν as a constant in contrast to the expected large range of variation in irregularity strength, $C_S L$.

In view of Eq. (4), constant ν translates to constant p , which was a Wideband post-processing observable. Investigation of the occurrence of p values observed at VHF from Poker Flat did show a rather narrow distribution (Fremouw and Lansinger, 1979), but the peak was between 2.0 and 2.5 rather than near 3, as expected. Further investigation showed that the value spread was not random but rather well ordered.

Figure 2 shows the mean value of p observed from Poker Flat as a function of geomagnetic L ($= \tan^2 \lambda_m + 1$). The peak near $L = 5.5$ (the value of the L shell passing through the receiving station) is believed to result from statistical nonstationarity as the line of sight scans rapidly through the region of geometrical enhancement in phase scintillation. For a certain identified application of the code, conservatism dictates erring on the high

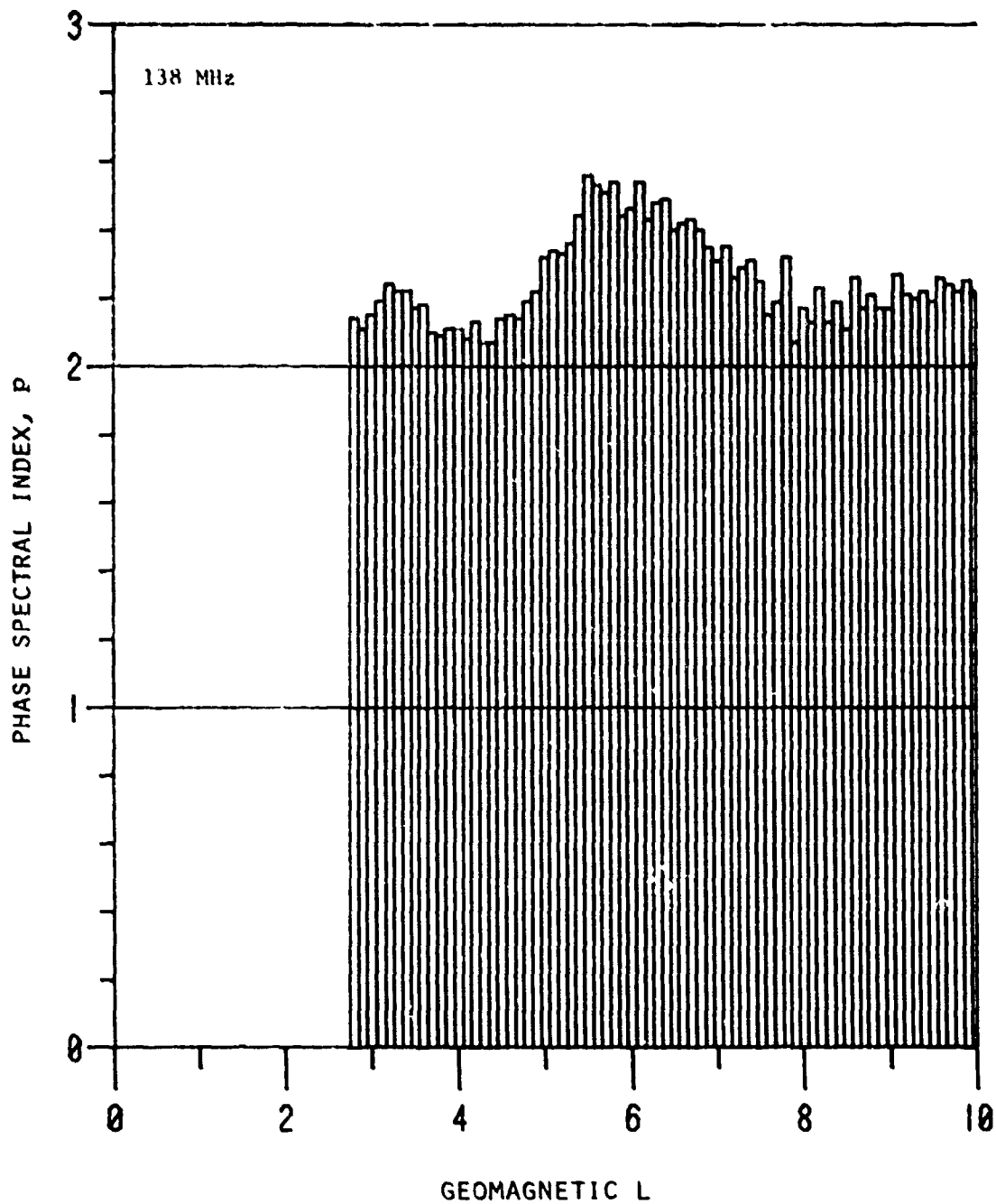


Figure 2. Relationship between VHF phase spectral index, p , and geomagnetic L value at the line-of-sight penetration point in the F layer. (After Fremouw and Lansinger, 1979.)

side if one is to employ a constant ν value in the face of the behavior disclosed in Figure 2. Doing so also tends to offset the effect of ignoring diffraction wrought by employing Eq. (4). Accordingly, the value of ν employed in WBMOD is 1.25 (i.e., $p = 2.50$).

With simple models established for outer scale, drift velocity, height, and gradient sharpness (spectral index) of the irregularities, we are ready to consider the more variable and, therefore, important parameters: a , b , and δ for describing the three-dimensional configuration of the irregularities and $C_p L$ for describing their height-integrated strength. The three remaining shape parameters have been established for auroral-zone irregularities by analyzing the geometrical behavior of scintillation as observed by means of Wideband at Poker Flat. The procedure and results are described in Section III B. By far the most effort was put into modeling irregularity strength, by means of iterative comparisons with the data, as described in Section III C.

B. THREE-DIMENSIONAL CONFIGURATION

Irregularities known *a priori* to have some degree of magnetic-field alignment are extended in a direction characterized by the dip angle, ψ . In a coordinate system thus tied to the geomagnetic field, the three-dimensional irregularity configuration is characterized by a , b , and δ . For isotropic irregularities, we would have $a = b = 1$, and geometrical control of scintillation would reduce to a path-length effect measured as $\sec \Theta$. "Rodlike" irregularities displaying axial symmetry about the magnetic field ($a > 1, b = 1$) would produce enhanced scintillation when the line of sight is nearly parallel to the field. Three-dimensionally anisotropic ($a > 1, b > 1$) irregularities produce enhanced scintillation near a line in the sky dictated by δ .

Pre-Wideband scintillation data clearly established field-alignment of the irregularities, with particularly large values of the along-field axial ratio, a , reported in the equatorial region (Koster, Katsriku, and Tete, 1966). It has now been established that the dominant irregularities immediately poleward of the nighttime high-latitude scintillation boundary are extended also in the geomagnetic east-west direction, as though layered like onion skins along L shells (Moorcraft and Arima, 1972; Singleton, 1973; Martin and Aarons, 1977; Fremouw et al, 1977b; Rino, Livingston, and Matthews, 1978). More recently, we have established that these so-called sheetlike irregularities are confined to the night side of the auroral irregularity zone (Fremouw, Lansinger, and Miller, 1980).

Alignment along L shells is described by $\delta = 0$, and we have coded such a constant value into WBMOD. (The value of δ is immaterial for axially symmetric irregularities, and the

only three-dimensionally anisotropic irregularities presently known to exist are L-shell aligned.) To establish initial values of a and b prior to the iterative adjustments to be described in Section III C, we performed the following analysis.

The entire available data base from Wideband passes over Poker Flat, which spans from late May 1976 to mid February 1979, was scanned for nighttime passes during which the line of sight came within 10° of the magnetic zenith. Using this criterion, 58 nighttime passes were identified as near-meridian passes, for which the field-line axial ratio, a, is the dominant geometrical factor that controls the strength of scatter. The distribution of measured phase-scintillation index, σ_ϕ , with angle off the local magnetic L shell at 350-km altitude, for these 58 passes, is shown in Figure 3, in which the geometrically-imposed enhancement at grazing angles to the L shell is very prominent. We quantified the prominence of this resonance-like enhancement by means of its width at $1/\sqrt{2}$ times the peak value of σ_ϕ . For instance, for the data shown in Figure 3, the enhancement width is 10° .

The geometrical enhancement for a given pair of a and b values can be calculated from Eqs. (5) and (6), together with representative pass geometry. Several such calculations were made, and the theoretical enhancement widths were scaled from the resulting plots of σ_ϕ vs. off-shell angle. Figure 4 shows the behavior of enhancement width with increasing a, for b fixed at 6, employing the geometry of nearly overhead daytime and nighttime passes. The observed enhancement width scaled from Figure 3 is plotted as an intersecting straight line.

Also shown in Figure 4 is the enhancement width scaled from a plot resembling Figure 3 but obtained from 44 daytime passes on which the line of sight came within 10° of the magnetic zenith. We noted that the enhancement width for near-overhead passes in the daytime was essentially the same as that for near-meridian passes at night and concluded that we could probably model a without diurnal variation. From the calculated curve in Figure 4 and the observed enhancement width of 10° , we inferred a value of 8.5 for a, subject to iterative refinement after establishing b.

Recent refinement of our analysis technique, being performed for geophysical research rather than for direct modeling purposes, suggests that there is some diurnal change in the value of a at the latitude of Poker Flat. This effect could result from a lesser degree of field alignment equatorward of the high-latitude scintillation boundary than poleward of it, however, since the boundary usually is located well poleward of Poker Flat during the day. Pending a possible future separation of latitudinal and diurnal variations of a, we have coded the following simple model for a:

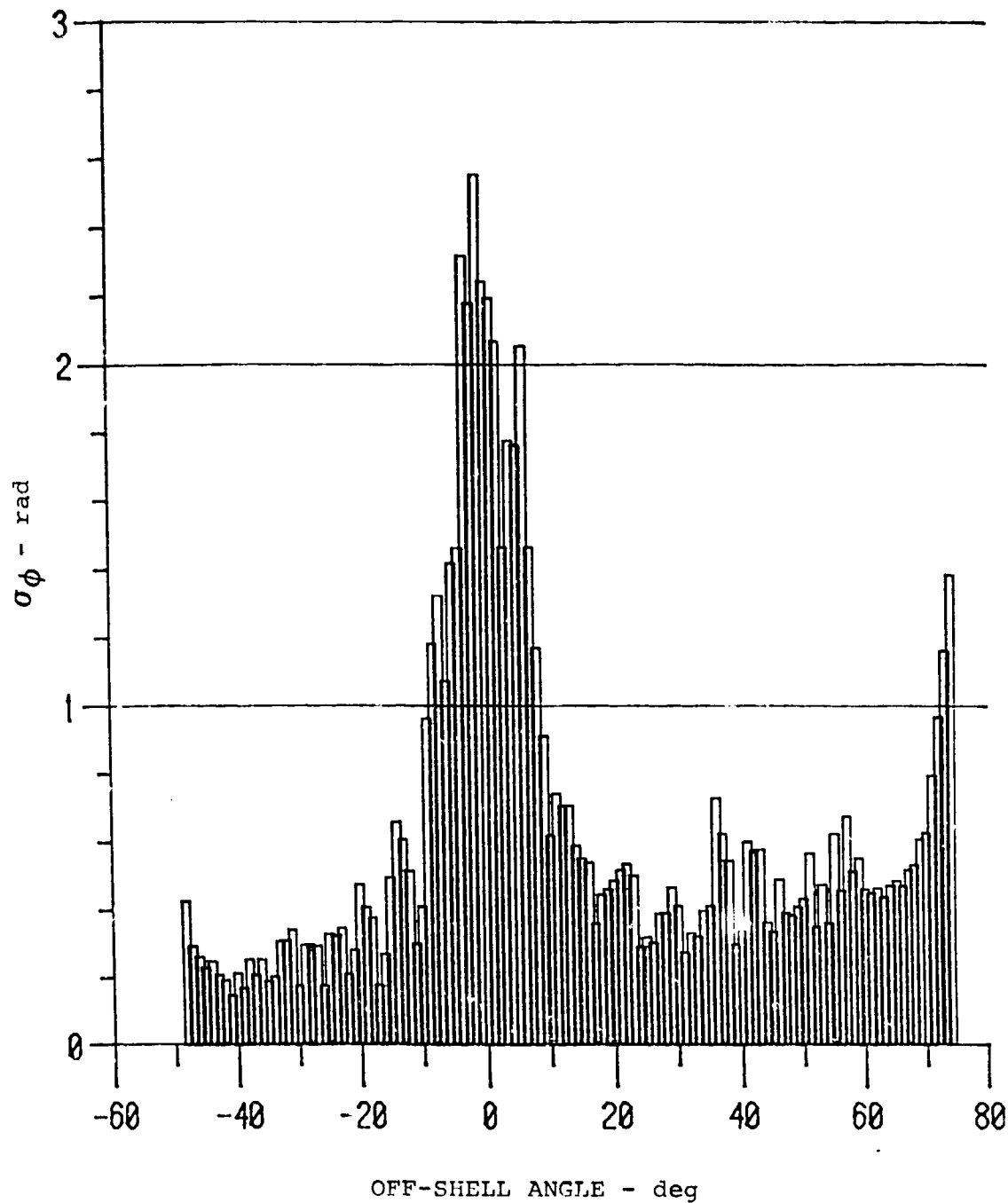


Figure 3. Observed distribution of phase-scintillation index, σ_ϕ , with angle between the line of sight and the local magnetic L shell for 58 nighttime passes nearly along the magnetic meridian.

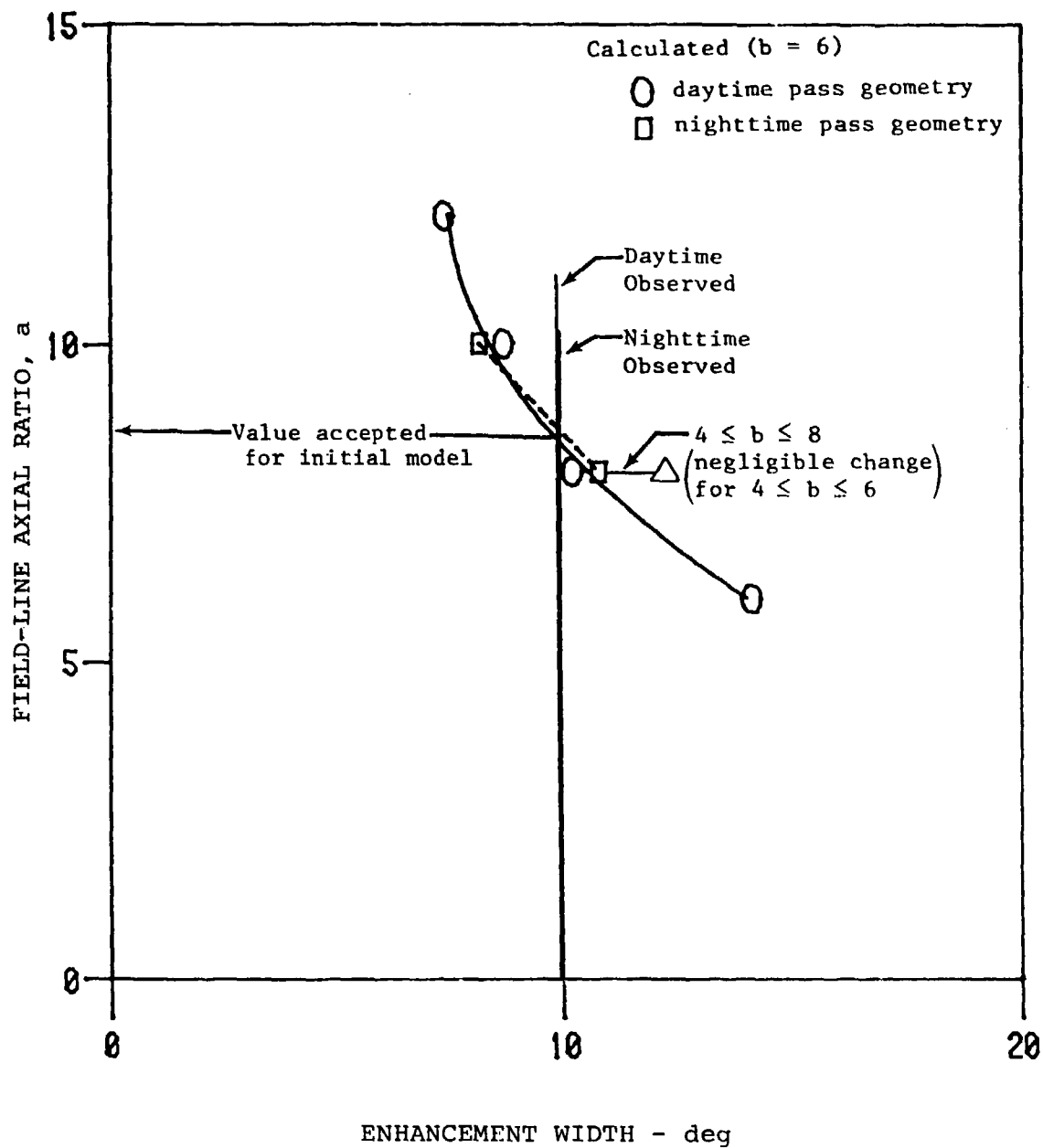


Figure 4. Relationship between field-line-axial ratio, a, and width of geometrical scintillation enhancement for nearly overhead passes, showing observed width and deduced value of a.

$$a = 30 - a_h \left(1 + \operatorname{erf} \frac{\lambda_m - 20^\circ}{3^\circ} \right). \quad (17)$$

Equation (17) describes very elongated irregularities near the geomagnetic equator and a field-aligned axial ratio of $30-2a_h$ elsewhere. Our initial value of a_h was based on Figure 4 and slightly modified by iterative tests to be described in Section III C.

Since b is the ratio of irregularity size in the magnetic east-west direction (along the L shell) to that in essentially the north-south (magnetic-meridian) direction (at high latitudes), its influence on the geometrical enhancement increases for off-meridian passes. Accordingly, we used passes to the east and west of Poker Flat for which the minimum angle between the line of sight and the local field line was at least 30° , to establish b . Again, we separated nighttime and daytime passes.

A scan of the nighttime data base revealed 86 passes between 0854 and 0939 UT to the east of the station and 85 passes between 1154 and 1234 UT to the west of the station that satisfied the minimum off-field angle criterion. The geometry of a pass near the center of each of these time windows was chosen for calculating the expected geometrical enhancement for several values of b , with the value of a fixed at 8.5. The minimum off-field angle for each of these passes was 43° , with the result that a and b have essentially equal influence on the enhancement and its angular width. It was for this reason that a was established first, using nearly overhead passes.

Figure 5 shows the calculated enhancement width as a function of b for the two representative pass geometries. Note that the difference in the geometry produces only about a degree of difference in enhancement width. Similar differences are produced by differences in specific pass geometry within the two time windows, as indicated by the horizontal uncertainty bars on the point calculated for $b = 6$.

The measured enhancement widths, scaled from histograms such as that shown in Figure 3, were 15.4° and 14.8° respectively for the easterly (pre-midnight) and westerly (post-midnight) data sets. These values are indicated on Figure 5 and correspond to b values of 4.5 and 5.3, respectively. The difference between the two is commensurate with the various uncertainties, but the consistently broader enhancement as compared with near-meridian passes does reveal that the average nighttime value of b at the geomagnetic latitude of Poker Flat is less than the value of a at the same latitude. We adopted $b = 5$ for the initial model. Note in Figure 4 that a change of b from 6, which was used in establishing $a = 8.5$, to the subsequently established b value of 5 does not measurably alter the deduced value of a .

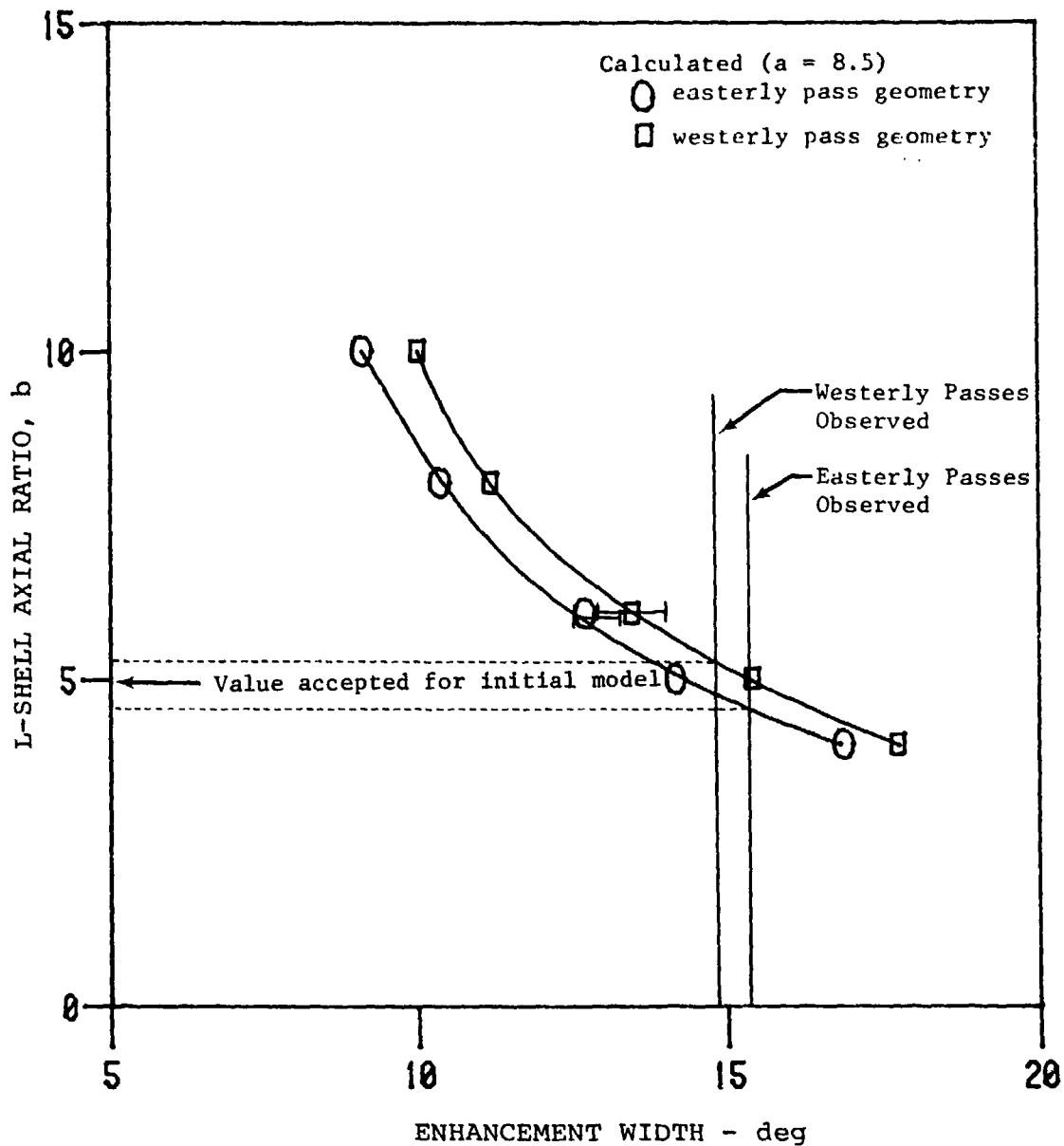


Figure 5. Relationship between L-shell axial ratio, b , and width of geometrical scintillation enhancement for nighttime passes to the east and west of Poker Flat, showing observed widths and accepted value of b . Horizontal uncertainty bars on $b = 6$ point indicate value spread calculated for range of geometries included in data sets employed.

It is commonly supposed that mid-latitude irregularities are axially symmetric ($b = 1$), but Wideband has shown that nighttime irregularities in the auroral precipitation zone are not ($b > 1$). The value of b established by the procedure described above is a kind of average nighttime value at the magnetic latitude of Poker Flat (65°), which often is near the scintillation boundary between the mid-latitude and auroral ionospheres at night.

Unlike the situation with a , for which refinement of technique has been necessary to uncover a possible diurnal variation, we have found clear evidence for such a variation in b . Taking all daytime data from the nonoverhead pass corridors together, we found no indication of geometrical enhancement. Again noting that such an effect might be caused by a latitudinal rather than a diurnal variation, we determined to separate passes during which the dayside scintillation boundary was (1) equatorward and (2) poleward of Poker Flat. Initially, we attempted a separation by K_p index, again finding no indication of nonoverhead enhancement for any range of magnetic disturbance.

We noted, however, the possibility that boundary sorting by K_p might not uniquely separate poleward and equatorward boundary locations. We undertook, therefore, to inspect pass-summary plots of σ_ϕ for all daytime passes of Wideband over Poker Flat (Fremouw, Lansinger, and Miller, 1980). So doing, we found close to one hundred passes in which the boundary could be identified with reasonable certainty as being equatorward of Poker Flat. In only three such passes was there a suggestion of possible geometrical enhancement well outside the overhead corridor. In no case was there truly convincing evidence. We concluded, therefore, that irregularities on the day side of the auroral ionosphere are rod-like, and we coded the following model for b :

$$b = 1 + b_h \left[1 + \cos \frac{\pi(T_m - 2)}{12} \right] \left[1 + \operatorname{erf} \frac{\lambda_m - \lambda_b}{\lambda_h} \right] \quad (18)$$

where T_m = geomagnetic time, in hours.

Equation (18) describes rodlike irregularities over most of the earth, with the exception of the region poleward of the nightside scintillation boundary latitude, λ_b . Above the boundary, the value of b changes smoothly from unity in the daytime to $4b_h + 1$ at night, peaking at that value 2 hours after geomagnetic midnight. The width of the latitudinal transition is described by λ_h , which will be discussed in Section III C. The initial value of b_h was set on the basis of Figure 5 and then modified by iteration, as will be discussed in the next section.

C. HEIGHT-INTEGRATED IRREGULARITY STRENGTH

The parameters discussed in the previous section are modeled in Subroutine MDLPRM of Program WBMOD. They leave only one of the eight irregularity parameters to be described. It is the most variable and, probably, the most important of the eight: the height-integrated strength, $C_s L$. The irregularity strength is modeled by means of Function CSL as follows:

$$\sqrt{C_s L} = E(\lambda_m, \lambda_g, T, D, \bar{R}) + M(\lambda_m, T) + H(\lambda_m, T_m, K_p, \bar{R}) \quad (19)$$

where λ_m = geomagnetic invariant latitude,
 λ_g = geographic latitude,
 T = local meridian time,
 D = day of the year,
 \bar{R} = smoothed Zurich sunspot number,
 T_m = geomagnetic time,
and K_p = planetary geomagnetic activity index.

The three terms in Eq. (19) respectively describe the strength of equatorial, mid-latitude, and high-latitude irregularities. The first two have not been tested extensively against Wideband data, and their development was not a part of the work carried out under this contract. We shall consider only the high-latitude term, H.

The high-latitude term is based on the observation that there often is a more-or-less abrupt boundary (Aarons, Mullen, and Whitney, 1969) between the mid-latitude region of relatively smooth ionosphere and the high-latitude scintillation region. It is located, typically, equatorward of discrete-arc auroras in the general vicinity of the diffuse auroral boundary. The underlying form of H stems from the supposition that the instantaneous boundary latitude is normally distributed about a mean value, λ_b , for a given set of T_m , K_p , and \bar{R} . This supposition, together with other considerations to be discussed shortly, yields the following form for H:

$$H = C_h(1 + C_r \bar{R}) \left[1 + \operatorname{erf} \left(\frac{\lambda_m - \lambda_b}{\lambda_h} \right) \right] \quad (20)$$

where the C's are constants to be established by iterative testing of the model against scintillation data, and where the error function arises from integration over the normal distribution of instantaneous boundary location, which distribution has standard deviation λ_h (Fremouw and Bates, 1971).

The multiplicative dependence of H on \bar{R} stems from (1) our observation at Poker Flat that scintillation increased with advancing phase of the solar cycle during the Wideband experiment (Fremouw and Lansinger, 1980) and (2) a consistent observation in the northern polar cap by Aarons (private communication). In contrast, scintillation activity in the polar cap seems rather unrelated to global magnetic activity, whereas the two are quite directly linked at Poker Flat. (We shall return to this point in discussing our model for the behavior of λ_b .) Moreover, we have found that scintillation activity is higher for a given K_p in years of high sunspot number than in years of lower \bar{R} (Fremouw, Lansinger, and Miller, 1980), so the dependence of H on K_p and \bar{R} may be modeled in separable fashion.

To establish the sunspot-number dependence of H, which is proportional to σ_ϕ through Eqs. (1), (7), and (19), we made a scatter plot of monthly averages of σ_ϕ against \bar{R} , as illustrated in Figure 6. Using nighttime data only, in order to minimize contamination from sub-boundary scintillation, we found the linear least-square fit shown in the figure. From the ratio of intercept to slope, C_r was evaluated as approximately 0.05. The linear fit describes the general upward trend of scintillation severity with increasing sunspot number rather well.

At the same time, there is an enticing quasi-cyclic departure of the observed behavior from the trend line. Since Basu (1975) found a marked seasonal dependence in scintillation activity in the Greenland sector, we investigated the possibility that the oscillatory behavior in Figure 6 may stem from a seasonal variation at Poker Flat. We found no statistically significant seasonal pattern, a point to which we shall return in Section V. We should like to explore the possibility that the departure from the linear trend is related to reversals in the interplanetary magnetic field, but such an investigation is beyond the scope of the present endeavor.

It is well known that the auroral oval and a variety of boundaries essentially concentric with it migrate equatorward with increasing geomagnetic activity and poleward with decreasing disturbance. The scintillation boundary participates in this migration and lies at a higher latitude on the day side of the earth than on the night side, as do the other boundaries. These facts about the scintillation boundary, together with the essential independence of polar-cap scintillation from K_p control, are described by Eq. (20) in conjunction with the following expression for the invariant latitude of the scintillation boundary:

$$\lambda_b = \lambda_1 - C_k K_p - C_{bt} \cos \frac{\pi(T_m - ?)}{12} \quad (21)$$

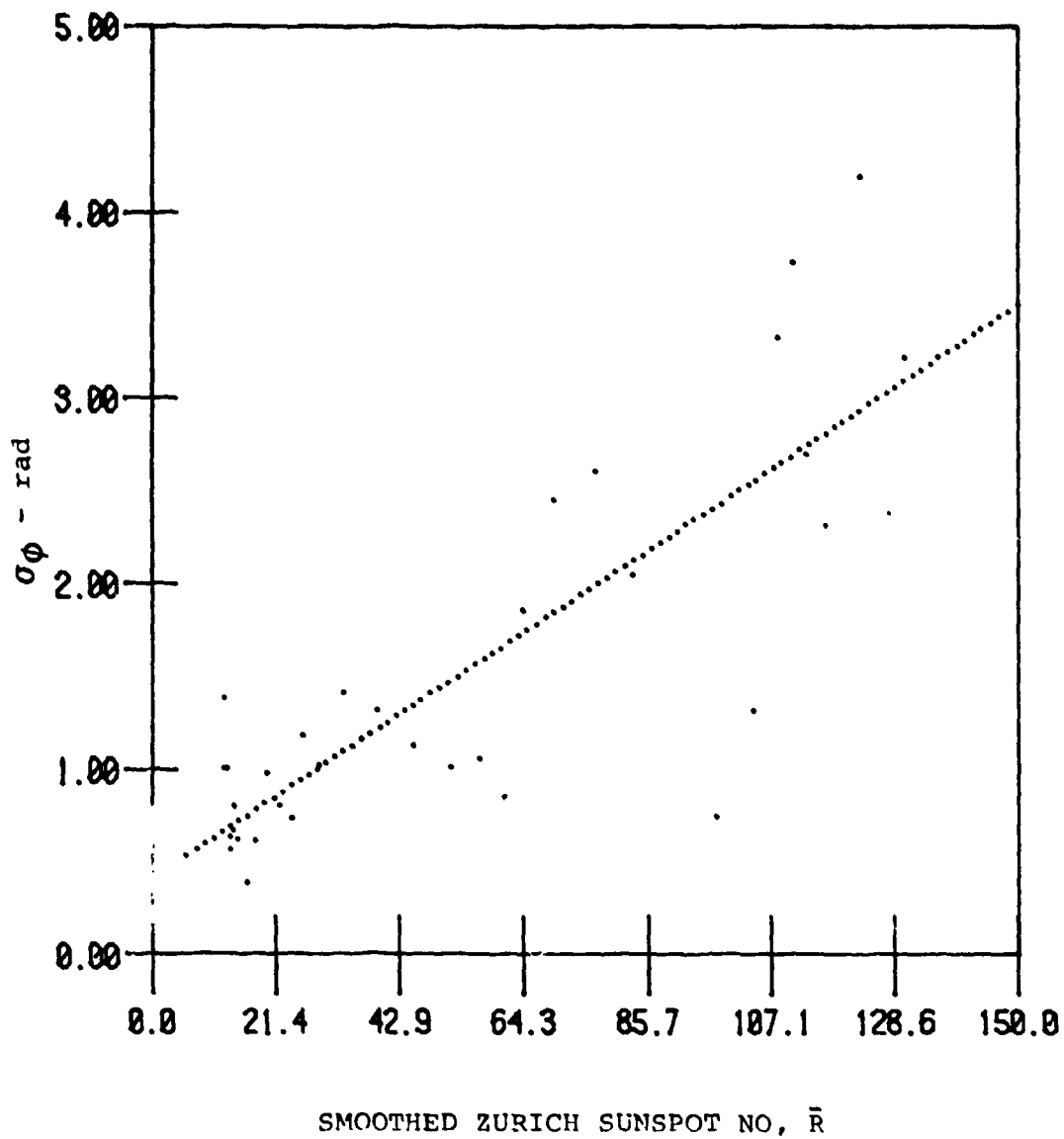


Figure 6. Sunspot-number dependence of nighttime, VHF phase-scintillation index at Poker Flat. Ordinate values represent monthly means.

where λ_1 and the C's are constants to be evaluated.

The remaining characteristic of the "average" or "climatological" scintillation boundary to be described is its width, λ_h (i.e., the latitudinal extent of the region over which, on average, scintillation severity changes from its low value in the sub-boundary "trough" to its high-latitude value). In the iterative testing to be described soon, we were able to obtain better fits to scintillation data by modeling the boundary as becoming more extended as it moves poleward. This does not necessarily imply that the instantaneous boundary is less steep when it is at higher latitude, and indeed Basu and Basu (private communication) report a rather steep boundary on the day side on the basis of *in-situ* plasma-probe data. Thus, our modeling experience may stem from a less strict ordering of boundary location with K_p on the day side than on the night side. Whatever the cause, we have found the following description of average boundary width to be useful:

$$\lambda_h = C_{hb} \lambda_b \quad (22)$$

where C_{nb} was found by iterative testing to be 0.15.

Equation (21) describes a circular scintillation boundary centered $\lambda_1 - C_k K_p$ degrees toward the dayside of the earth from the geomagnetic pole. The line of symmetry passing through the pole, however, is not the geomagnetic-midnight meridian, but rather is shifted two hours after midnight. This shift is based on a finding of Basu and Basu (1981) from *in-situ* plasma-probe data, which provide more continuous time coverage than does the Wideband data population. (Scintillation and *in-situ* data are complementary in a number of respects, the latter not providing any information on three-dimensional configuration of the irregularities, for instance.) We found that imposing such a shift in Eqs. (18) and (21) increased our ability to obtain simultaneously satisfactory fits to some of the iterative-test data sets to be discussed next.

The bulk of our modeling effort involved establishing the utility of Eqs. (17) through (22) and, more particularly, evaluating the constants that give them quantitative meaning. Our procedure was one of iterative testing against VHF measurements of σ_ϕ from Poker Flat. The model contained in Program IONSCNT (Fremouw and Rino, 1978) contained a fifth term in the counterpart of Eq. (19), intended to describe an additive scintillation contribution associated with discrete auroras. In individual Wideband passes, one does observe localized regions of scintillation (most notably of phase), usually to the north of Poker Flat, that are reminiscent of auroral arcs. During the course of iterative testing, however, we found it unnecessary and cumbersome to account for these features explicitly in

an "average" model. Apparently, their location is sufficiently variable (and their prominence sufficiently infrequent) that they simply contribute unobtrusively, on average, to the high-latitude scintillation described by the H term of Eq. (19).

Attempts to retain the fifth term, and simultaneously to decrease the height of the modeled scattering layer in order to account for an E-layer contribution in the region of discrete-auroral contribution, complicated the modeling without improving fits to phase-scintillation data. It may be that modeling on the basis of S_4/σ_ϕ would reveal such a contribution, but we were not able to pursue such a possibility in the present work. Thus the C_gL model in WBMOD contains only the four terms included in Eq. (19), with the quantifying constants iteratively set to match phase-scintillation observations by the following procedure.

Inspection of Eqs. (17), (18), (20), (21), and (22) reveals the following eight constants to be established for quantitative description of the three-dimensional configuration and height-integrated strength of high-latitude scintillation-producing irregularities: a_h , b_h , C_h , C_r , λ_1 , C_k , C_{bt} , and C_{hb} . Fortunately, as has already been discussed in Section III B and earlier in this section, essentially deductive procedures were found for establishing at least starting values for four of the eight: a_h , b_h , C_r , and C_{hb} . Starting values for the remaining four were available from IONSCNT and from an experience-based intuition about behavior of the high-latitude ionosphere.

With starting values for the eight iterative constants established, the Wideband data population from Poker Flat was divided into 22 subsets, 14 of which were used for iterative model-building, with the remaining eight reserved for final testing. The division was made on the basis of pass corridor and K_p . Since Wideband is in a sun-synchronous orbit, pass corridors established for defining geometry could be parameterized by means of pass time. The first two corridors to be defined were (1) nighttime passes for which the pass-minimum value of the angle between the propagation vector and the geomagnetic field was 10° or less and (2) daytime passes meeting the same criterion. These two corridors turned out to be bounded in universal time (UT) by (1) 1018-1059 and (2) 1944-2022.

Local standard time at the station corresponds to UT - 10 hours. Following definition of the foregoing two overhead corridors, corridors well east (earlier in time) and well west (later in time) of the station were defined for iterative modeling. They are bounded in UT respectively by (night) 0854-0939 and 1154-1239 and by (day) 1739-1824 and 2039-2124. For both day and night, final-test corridors were defined between the overhead and east corridors and between the overhead and west corridors. They are designated as east-intermediate and west-intermediate, and data from them were not used in iterative model

building but rather were used as an indication of model fidelity after all iterative constants were frozen. Some passes occurred outside the foregoing ten corridors, in corridors designated as (nighttime) low east, northwest and (daytime) northeast, low west. These corridors were relatively sparsely populated, and data from them were not used in model development or testing.

Once the six geometry/time corridors to be used in model-building and the four to be used for final test were established, the data in them were divided into the following three K_p ranges: 0 through 2+ (designated low), 3- through 5+ (mid), and 6- and above (high). For the low and mid categories of K_p , sufficient data exist for separation into all geometry/time corridors. There were too few high- K_p passes, however, to make statistically meaningful data subsets by corridor. Thus for high K_p , only two subsets were established (one for daytime and one for nighttime). Finally, then, there were 14 data subsets for iterative modeling (six each daytime and nighttime corridors for each of two K_p ranges plus two high- K_p sets) and eight for final testing (two each daytime and nighttime corridors for each of two K_p ranges).

For each geometry corridor, a representative pass was selected from near the center of the corresponding UT range. The pass time and the beginning and ending latitude and longitude for the representative pass were then input to WBMOD, and the code was run in ORBT mode. External software was employed to display the calculated value of σ_ϕ as a function of invariant latitude of the F-layer (350-km) penetration point on a graphics terminal (Tektronix 4025). The values of σ_ϕ measured during passes in each data subset were then sorted into the same penetration-point latitude bins, and their average values also were displayed on the screen.

For the WBMOD calculations, K_p was set at the middle value (1, 4, or 7) of the range included in the data subset being used for comparison. For all iterative modeling runs, the sunspot number was fixed at 50, which was set after calculating 52 as the mean value encountered in the Wideband experiment (weighted by the number of data points available for each incremental value of \bar{R}). Sunspot-number dependence was modeled independently, as discussed in conjunction with Figure 6.

With the independent variables (geometry, time, K_p and \bar{R}) set, WBMOD was run and the result compared graphically with the corresponding σ_ϕ measurements from a given data subset. The model constants were adjusted to provide better (subjectively judged) fits for each representative pass. Initially, such iterations were performed for the low- K_p and mid- K_p data sets for each of the six nighttime model-building corridors. With interim values for the constants set, a similar round of iterations was performed for the daytime cases. Several iterations often were run at a single modeling session, comparisons being made with

a number of data subsets. Periodically, hard-copy plots of all 12 passes were made so as to permit simultaneous comparison of data and model results for all. Such comparisons yielded strategy for the next iteration session. The objective was to find a set of constants which simultaneously gave satisfactory fits for all 12 subsets plus the two high- K_p sets.

First iterations with the high- K_p sets were discouraging, the model generally overstating the level of VHF phase scintillation. As a result of other related work, however, a deficiency in the Wideband VHF data population was found. Inspection of pass-summary data from very active passes revealed breakdown of the linear wavelength dependence of σ_ϕ predicted by the phase-screen theory and otherwise observed. The breakdown invariably took the form of a saturation in the measured VHF value. As a result of some early experience with equatorial Wideband data, we suspect that the effect results from an inability of either the Wideband receivers or, more likely, routine data-processing procedure to track large and rapid phase excursions.

Whatever the source of breakdown in the wavelength dependence of reported σ_ϕ values, it precludes interpreting the VHF data by means of the phase-screen theory of Rino (1979a) to deduce characteristics of ionospheric irregularities, which is the essence of our modeling procedure. Accordingly, we reprocessed the entire Wideband summary data base from Poker Flat, substituting scaled UHF (or, in few instances, L-band) data for the "saturated" VHF values of σ_ϕ . As described in detail by Fremouw, Lansinger, and Miller (1980), our method was tantamount to selecting the lowest frequency for which the phase-screen theory was demonstrated to be valid. This turned out to be VHF for 90% of the 35,223 measurements in the population, UHF for 8%, and L Band for 2%. (A modest 247 points were totally rejected by our procedure.) Our final iterative model-building and testing were performed with the reconstituted data population.

Lest the reader be concerned that we have manipulated our data to fit theory, let us re-emphasize the task at hand. It was to characterize ionospheric irregularities in terms of equations coded into Subroutine MDLPRM and Function CSL, using the phase-screen theory coded into Subroutine SCNT3 and GEOFAC. For this purpose, we must use data obtained under conditions for which that scattering theory is valid. What we did was to select data from a sufficiently high frequency that the theory was found to be valid by systematic test. If, indeed, the phase-screen theory breaks down under severe scintillation conditions, then WBMOD results will not be valid at VHF under such conditions. The underlying irregularity model is not brought into question thereby, however, and the code output will be valid at higher frequencies. In point of fact, we believe it more likely that the Wideband data-processing procedures were overwhelmed than that the phase-screen theory broke down, but we have not proven this conjecture.

Once we returned to iterative testing after reconstitution of the VHF data base, we obtained acceptable high- K_p fits simultaneously with fits at low and mid K_p with relative ease. As related earlier, the solar-cycle constant, C_r , was not changed during iteration. It was anticipated that a_h and b_h would have to be increased somewhat from their initial values. This was expected because the values of a and b deduced from Figures 5 and 6 represent a kind of average value at the geomagnetic latitude of Poker Flat. If Eqs. (17) and (18) completely describe the latitudinal behavior of a and b , then a_h and b_h must be chosen to produce values of a and b well poleward of the boundary that are somewhat larger than the values encountered at the latitude of Poker Flat, which is crossed by the boundary in its migrations.

The deduction of 8.5 and 5 for a and b at Poker Flat's latitude, however, was performed without regard to latitudinal variation of $C_g L$. The iterative procedure, on the other hand, permits simultaneous consideration of the behavior of the axial ratios and the strength (albeit on a less deductive basis). The iterative procedure produced a and b values of 8 and 4 well poleward of the boundary and, therefore, somewhat lower average values at Poker Flat's latitude.

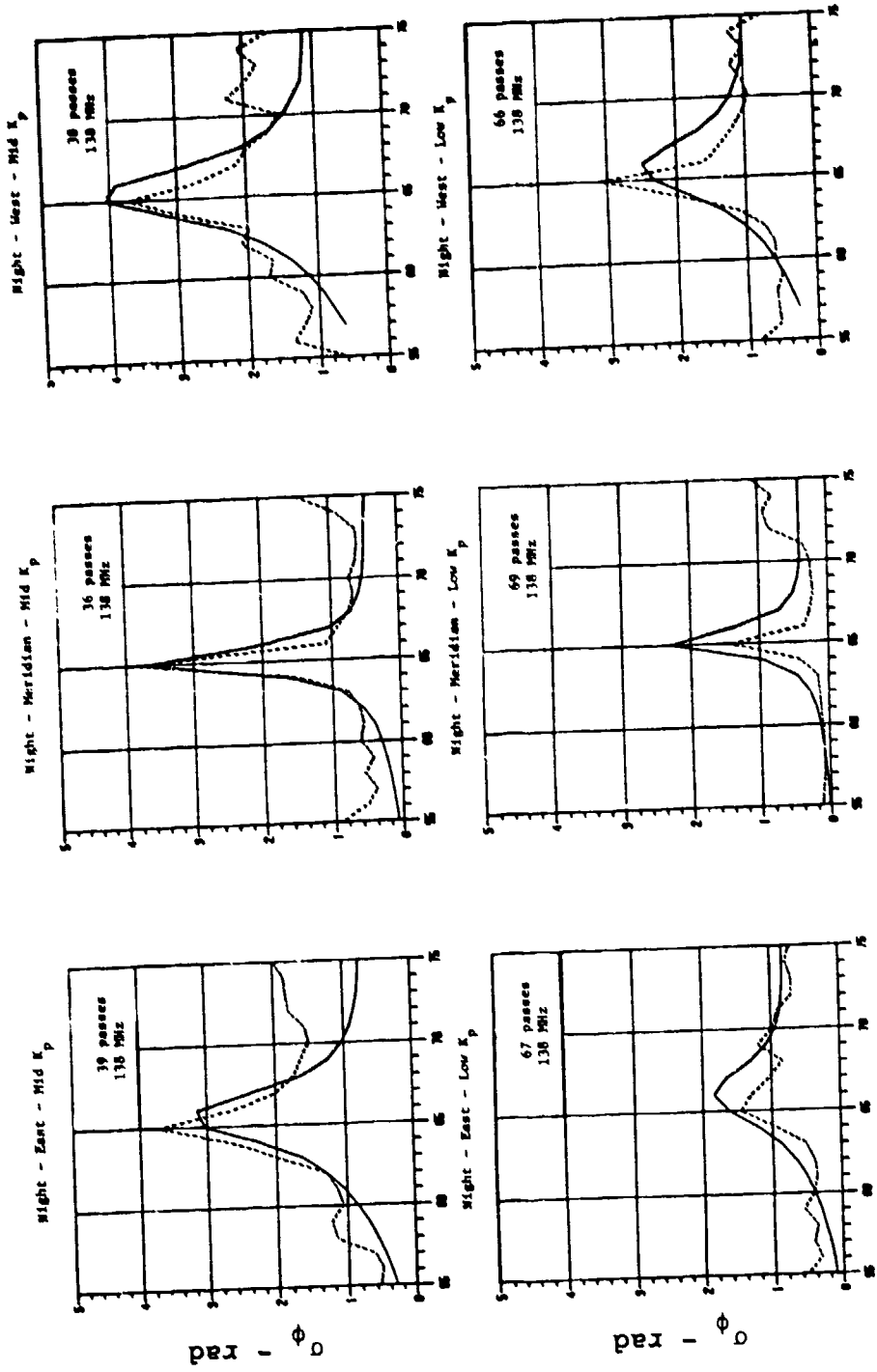
The final values iteratively established for the high-latitude model constants are as follows:

$$\begin{array}{llll}
 a_h = 11 & C_h = 4.3 \times 10^{11} & \lambda_1 = 71^\circ & C_{bt} = 5.5 \\
 b_h = 0.75 & C_r = 0.0496 & C_k = 1.5 & C_{hb} = 0.15
 \end{array}$$

The resulting model outputs are compared with their data counterparts in Figures 7, 8, and 9.

Figure 7 contains the six low- K_p (bottom) and mid- K_p (top) nighttime representative passes (solid) and data subsets (broken). From left to right, the passes progress in time (and the orbital plane from east to west). The geometrical enhancements are prominent in both the calculations and the data sets, being located close to the latitude of the station, at the point of minimum off-shell angle (subject to one-degree latitude resolution). The general increase in activity with increasing K_p is evident, and the differences in enhancement between overhead and off-meridian passes and between pre-midnight and post-midnight passes are reasonably well reproduced by the model.

In some instances, the model underestimates σ_ϕ to the north of the station. The calculated value there is depressed by a decrease in V_e as the line of sight scans along extended axes of either rodlike or sheetlike irregularities. It is tempting to introduce a further latitudinal change in axial ratios (decreasing at higher latitudes) in an attempt to improve the fits. There is insufficient information for reliably doing so, however, from



INVARIANT LATITUDE - deg

Figure 7. Comparison of nighttime, VHF phase scintillation index calculated (solid) by means of Program WBMOD and observed (broken) at Poker Flat, Alaska in the Wideband Satellite Experiment. Left: pre-midnight passes to the east of the station. Center: near-midnight passes essentially along the geomagnetic meridian. Right: post-midnight passes to the west of the station. Bottom: $0 \leq K_p \leq 2+$, Top: $3 \leq K_p \leq 5+$. No. of passes in each data set is indicated in the upper righthand corner of each grid. Calculated values are for a single representative pass.

the phase data only. Improvements may well be possible on the basis of S_4/σ_ϕ , but such an effort was beyond the scope of the present work.

Results for daytime passes in the overhead (left) and west (right) corridors are displayed in Figure 8. The east corridor produced rather short passes and did not contribute appreciably to the iterative modeling. Again, the low- K_p sets are at the bottom and the mid- K_p sets are at the top. The total lack of a geometrical enhancement in the west corridor attests to the diurnal variation in b , describing L-shell alignment at night and axial symmetry (in view of the enhancement in the overhead corridor) in the daytime. The general level of scintillation is reasonably well reproduced, as it was at night.

The code overestimates daytime scintillation somewhat to the north of the station in several instances. The gratifying degree of fit in the west corridor under mid- K_p conditions, however, suggests reasonable fidelity in the latitudinal description of irregularity strength. This case is useful for that purpose because the transition region is accessible from Poker Flat, and because complications regarding axial ratios do not arise in this geometry.

Finally, the high- K_p results for nighttime and daytime are shown in Figure 9. For very disturbed conditions ($K_p \geq 6$), there were too few Wideband passes to maintain separation of the data population into subgroups by geometry/time corridors. Geometrical and time considerations were taken into account in the model calculations in the following way. First, the number of high- K_p passes in each corridor was established, along with the average sunspot number and K_p value for that small data subset. The code was then run for the previously chosen representative pass geometry and time for that corridor, using the subset-average values of \bar{R} and K_p . The resulting σ_ϕ values in each latitude bin then were averaged together after weighting by the number of data passes in each corridor. What appears in Figure 9 as solid curves are these average calculation results for nighttime (left) and daytime (right) independently, together with (broken curves) the observed averages from the corresponding data sets.

The results illustrated in Figure 9 were used in the few final iterations of the model constants, but far less so than the data contained in Figures 7 and 8. In particular, the rather satisfactory fit to the nighttime data in Figure 9 poleward of Poker Flat was obtained with very little high- K_p -based iteration. The overestimation of nighttime σ_ϕ in the geometric-enhancement region probably is overstated in Figure 9. The data-editing procedure we used for identification of saturated values in the VHF data population is based on comparison with a threshold value for the wavelength dependence of σ_ϕ . Thus, under extreme conditions, some moderately saturated values most likely were retained in the data population. The calculated peak, therefore, may be a better representation than the observed-data curve would indicate.

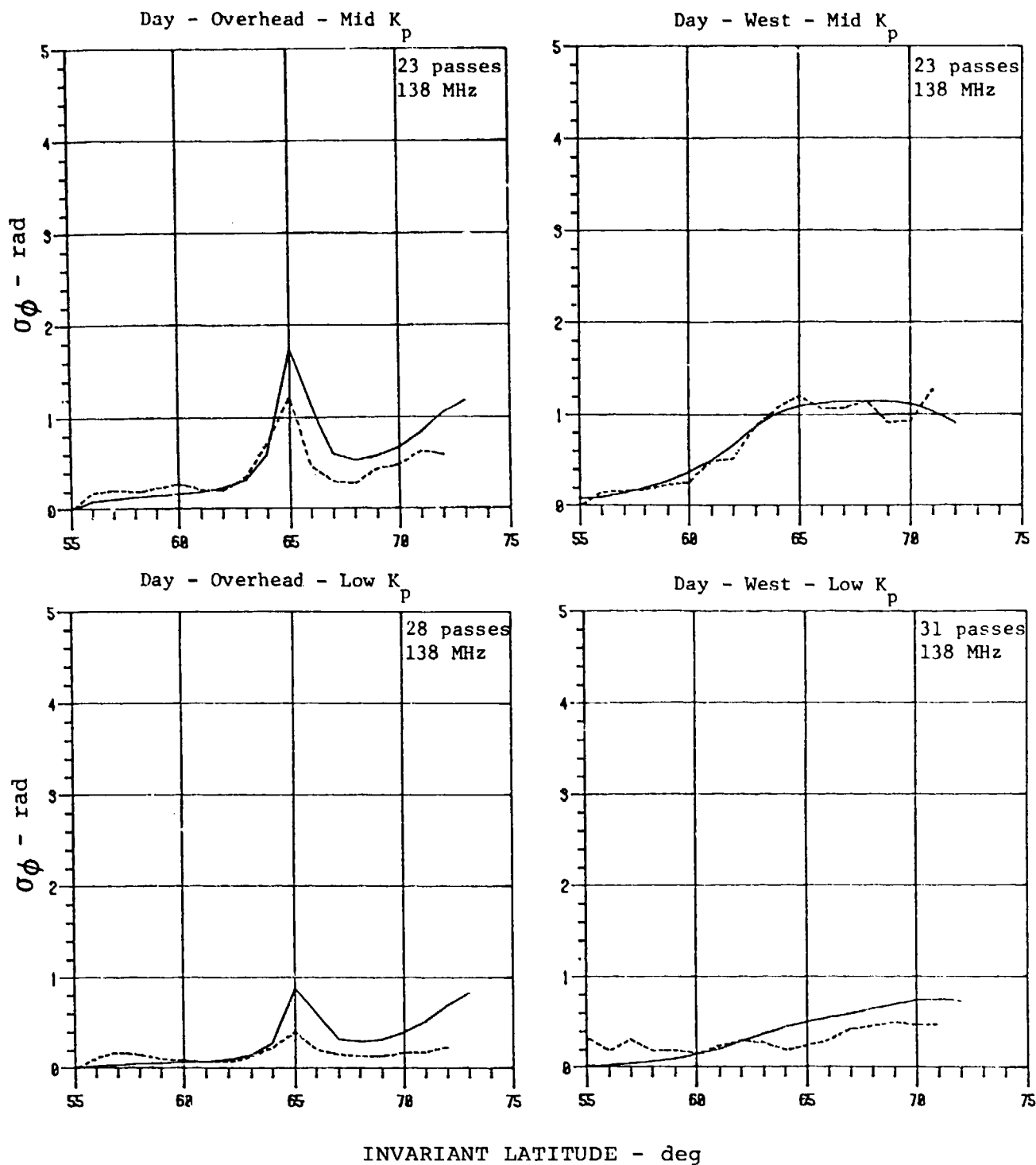


Figure 8. Comparison of WBMOD (solid) results and observed values (broken) of daytime VHF phase scintillation index. Left: overhead (morning) passes. Right: west (late morning) passes. Bottom: $0 \leq K \leq 2+$. Top: $3 \leq K \leq 5+$. No. of passes is indicated in the upper righthand corner of each grid.

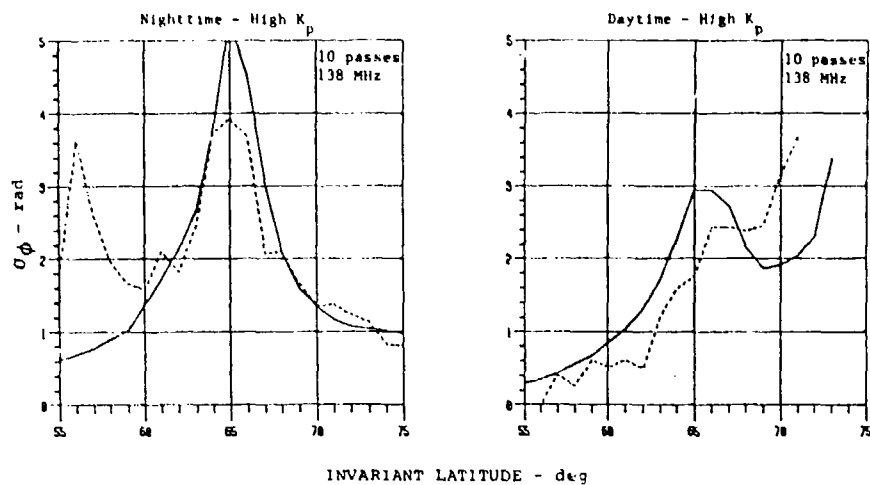


Figure 9. Comparison of model results (solid) and observed values (broken) of VHF phase scintillation index for geomagnetically very disturbed ($K_p \geq 6$ -) nighttime (left) and daytime (right) conditions.

The most striking and potentially significant deficiency in the nighttime model lies well equatorward of Poker Flat. In several instances, unexpectedly strong phase and intensity scintillations were observed under magnetically disturbed conditions at an ionospheric penetration latitude of about 56° invariant. Quite likely representing a signature of some form of convective instability at the plasmopause, this scintillation feature is totally unaccounted for in the present model. An effort to do so has been proposed to DNA by Physical Dynamics (Fremouw, 1980b).

The general level and latitudinal distribution of daytime scintillation under high- K_p conditions seems rather well described by the model. Figure 9 is consistent with the idea, however, that there may be a diurnal variation in the field-aligned axial ratio, a , which is not described by the present model. As discussed in Section III B, systematic analysis has disclosed a smaller average value of a at the latitude of Poker Flat in the daytime than at night, but insufficient data were available to sort out reliably whether the effect stems from a diurnal variation or from different values of a poleward and equatorward of the scintillation boundary. Figure 9 is consistent with the former view. Unlike the results shown in Figures 7 and 8, those in Figure 9 include passes from intermediate corridors. They contribute to the geometrical enhancement indicated in the daytime model result shown in Figure 9, and they are sensitive to the modeled value of a . Data from a higher latitude station are needed to do a fully satisfactory job of modeling dayside auroral scintillation.

IV. USE OF THE CODE

Program WBMOD is structured for interactive application from a user terminal. A sample interaction is provided in Table 2, in which system queries are indicated in caps and user responses in lower case. As indicated in the table, a computation session begins with a request by the code for a label by which the run output is to be identified. The label may consist of any alphanumeric string of up to 40 characters. The code then permits the user to make several choices, including whether or not to rely upon two relatively rudimentary aspects of the model, which were discussed in Section III A.

First, the user selects either one-way (communication system) or two-way (radar) propagation and then the reciprocal of the low-frequency cutoff of the band of phase-fluctuation frequencies to which his system is susceptible, which is used as f_0 in Eq. (7) or (9a). Thereafter, he either provides values for the geomagnetic east-west outer scale of the *in-situ* electron-density spectrum and for the drift velocity of ionospheric irregularities or elects to let the code employ default values for them. (See the definition of outer scale following Eq. 8 on p. 10.)

Next, the code requests initial values for 11 potentially variable parameters that describe the operating scenario. Once the initial values have been set by the user, the code inquires as to which computational mode is desired. The user may select any of the 11 parameters just initialized to be the independent variable against which output parameters are to be tabulated. Alternatively, either the receiver (radar target) or transmitter (radar) may be stepped in latitude (north positive) and longitude (east positive) along a great circle by typing in RCRD or TCRD, respectively, instead of a single variable name.

In all of the foregoing modes, scintillation parameters are calculated for each incremented value of the independent variable(s) without introducing a line-of-sight scan. (That is, scintillation is taken to arise only from irregularity drift.) Finally, the ORBT mode may be selected, in which the receiver or transmitter (whichever is higher) moves along a constant-altitude, circular orbit, and scintillation results from a combination of line-of-sight scan and irregularity drift. (In most low-orbiting applications, the former velocity dominates.) Whatever mode is chosen, the code now asks for the final value(s) of the changing parameter(s) and for the number of increments desired between the initial and final values.

A sample output, corresponding to the interaction contained in Table 2, is illustrated in Table 3. Following a general heading, the title specified by the user is printed. Thereafter, his input parameters are identified, followed by the calculation outputs. The first output is a single printing of the power-law spectral index, p , of phase scintil-

Table 2
Sample Input Interaction Between WBMOD and User

WBMOD REQUESTS A LABEL FOR THIS RUN.

p9-50 simulation

DO YOU WANT ONE-WAY (1) OR TWO-WAY (2) PROPAGATION?

1

STATE DURATION (IN SEC) OVER WHICH SYSTEM REQUIRES PHASE STABILITY (0.0 FOR SYSTEMS NOT SENSITIVE TO PHASE SCINTILLATION)

10.0

ESTIMATE IONOSPHERIC OUTER SCALE (KM OR TYPE "MODEL" FOR EFFECTIVELY INFINITE DEFAULT VALUE).

model

ESTIMATE IRREGULARITY DRIFT VELOCITY (IN M/S FOR GEOMAGNETIC NORTH, EAST, DOWN OR TYPE "MODEL" FOR KP-DEPENDENT DEFAULT VALUE).

-100.0, 500.0, 0.0

PROVIDE INITIAL VALUES FOR FOLLOWING (IN MHZ, DECIMAL NUMBER, HOURS, DEG, OR KM, AS APPROPRIATE):

OPERATING FREQUENCY (FREQ): 137.68

PLANETARY GEOMAGNETIC ACTIVITY INDEX (FKP): 4.

SMOOTHED ZURICH SUNSPOT NUMBER (SSN): 50.

DAY OF THE YEAR (DAY): 150.

MERIDIAN TIME AT RECEIVER OR AT RADAR TARGET (TIME): 2.4407

LATITUDE OF RECEIVER OR TARGET (RLAT): 65.13

LONGITUDE OF RECEIVER OR TARGET (RLON): -147.49

ALTITUDE OF RECEIVER OR TARGET (HR): 0.195

LATITUDE OF TRANSMITTER OR RADAR (TLAT): 80.404

LONGITUDE OF TRANSMITTER OR RADAR (TLON): -82.718

ALTITUDE OF TRANSMITTER OR RADAR (HT): 1026.

SELECT CHANGING PARAMETER (ONE OF NAMES IN PARENS ABOVE OR TYPE "RCRD" OR "TCRD" TO STEP RECEIVER OR TRANSMITTER ALONG GREAT CIRCLE OR "ORBT" TO CAUSE HIGHER TERMINAL TO PERFORM ORBITAL SCAN AT CONSTANT ALTITUDE).

orbt

PROVIDE FINAL VALUES FOR FOLLOWING:

LATITUDE OF TRANSMITTER (TLAT): 53.033

LONGITUDE OF TRANSMITTER (TLON): 177.546

SPECIFY NUMBER OF CALCULATION INCREMENTS (# OF POINTS - 1): 50

Table 3. Sample WBMOD Output.

F-LAYER-PRODUCED RADIOWAVE SCINTILLATION

 CALCULATED FROM A MODEL DEVELOPED BY PHYSICAL DYNAMICS, INC.
 BELLEVUE, WA 98009

THIS RUN IS F9-50 SIMULATION

ONE-WAY PROPAGATION

REQUIRED PHASE-STABILITY DURATION = 10.0 SEC

IONOSPHERIC OUTER SCALE: EFFECTIVELY INFINITE

IRREGULARITY DRIFT VELOCITY:
 -100.000 M/S NORTH 500.000 M/S EAST 0.000 M/S DOWN

FREQ = 137.68 MHZ KP INDEX = 4.0 SSN = 50 DAY OF YEAR = 150

TIME = 2.44 HOURS LMT AT RECEIVER
 FOR FIRST ORBIT POINT

RECEIVER COORDINATES TRANSMITTER COORDINATES
 LAT = 65.13 DEG LAT = 80.40 DEG
 LON = -147.49 DEG LON = -82.72 DEG
 ALT = 0.195 KM ALT = 1026.000 KM

FOR THIS RUN, THE CHANGING PARAMETERS WERE:
 TRANSMITTER LATITUDE AND LONGITUDE ALONG ORBIT

POWER-LAW SPECTRAL INDEX OF PHASE SCINTILLATION: P = 2.50

	TLAT	TLOn	T	RMS PHASE(RAD)	S4
1	80 398	-82 705	0.3989E-01	1.297	0.49398
2	80 627	-87.312	0.3684E-01	1.247	0.48530
3	80.775	-92.115	0.3473E-01	1.210	0.47652
4	80.899	-97.099	0.3318E-01	1.183	0.46770
5	80.937	-102.079	0.3214E-01	1.164	0.45889
6	80 908	-107.103	0.3141E-01	1.151	0.45015
7	80 812	-112.061	0.3084E-01	1.140	0.44157
8	80 652	-116.885	0.3051E-01	1.134	0.43321
9	80.431	-121.520	0.3045E-01	1.133	0.42519
10	80.152	-125.924	0.3052E-01	1.134	0.41761
11	79.822	-130.071	0.3080E-01	1.140	0.41058
12	79.443	-133.945	0.3127E-01	1.148	0.40424
13	79.023	-137.544	0.3194E-01	1.160	0.39874
14	78.564	-140.874	0.3281E-01	1.176	0.39425
15	78.072	-143.946	0.3405E-01	1.198	0.39099
16	77.550	-146.775	0.3565E-01	1.226	0.38918
17	77.002	-149.380	0.3766E-01	1.260	0.38917
18	76.432	-151.778	0.4043E-01	1.306	0.39127
19	75.841	-153.988	0.4378E-01	1.359	0.39593
20	75.233	-156.026	0.4816E-01	1.425	0.40372
21	74.609	-157.909	0.5390E-01	1.508	0.41532
22	73.972	-159.592	0.6160E-01	1.612	0.43159
23	73.322	-161.267	0.7152E-01	1.737	0.45357
24	72.651	-162.769	0.8537E-01	1.897	0.48247
25	71.991	-164.167	0.1041E 00	2.095	0.51765
26	71.313	-165.470	0.1300E 00	2.341	0.56625
27	70.626	-166.690	0.1657E 00	2.643	0.62268
28	69.933	-167.832	0.2150E 00	3.011	0.68724
29	69.233	-168.903	0.2787E 00	3.428	0.75462
30	68.528	-169.914	0.3508E 00	3.846	0.81517
31	67.818	-170.865	0.4110E 00	4.163	0.85817
32	67.104	-171.763	0.4292E 00	4.354	0.87716
33	66.385	-172.612	0.3928E 00	4.070	0.87173
34	65.662	-173.418	0.3207E 00	3.677	0.84481
35	64.936	-174.183	0.2451E 00	3.215	0.80173
36	64.207	-174.910	0.1807E 00	2.760	0.74953
37	63.475	-175.603	0.1330E 00	2.368	0.69457
38	62.740	-176.264	0.9788E-01	2.031	0.64092
39	62.003	-176.896	0.7273E-01	1.751	0.59041
40	61.263	-177.500	0.5433E-01	1.514	0.54337
41	60.521	-178.079	0.4098E-01	1.315	0.49941
42	59.777	-178.635	0.3078E-01	1.139	0.45785
43	59.032	-179.170	0.2315E-01	0.988	0.41798
44	58.285	-179.684	0.1730E-01	0.854	0.37924
45	57.536	-179.821	0.1277E-01	0.734	0.34124
46	56.786	-179.344	0.9283E-02	0.626	0.30378
47	56.035	-178.883	0.6402E-02	0.528	0.26691
48	55.282	-178.437	0.4882E-02	0.440	0.23089
49	54.528	-178.006	0.3074E-02	0.360	0.19619
50	53.773	-177.589	0.1997E-02	0.290	0.16335
51	53.017	-177.184	0.1239E-02	0.229	0.13301

lation. Finally, columns containing the following information are provided: calculation point number; changing parameter(s); the spectral strength parameter, T, for of phase scintillation; the phase scintillation index, σ_{ϕ} ; and the intensity scintillation index, S_4 .

V. CONCLUSION

Program WBMOD combines the most useful scattering theory available for calculating radiowave scintillation with the best available description of the electron-density irregularities responsible for ionospherically produced scintillation. The theory is based on the equivalent phase-screen representation of Booker, Ratcliffe, and Shinn (1950), formulated to account for three-dimensionally anisotropic irregularities (Singleton, 1970) described by a power-law spatial spectrum. The formulation employed was developed by Rino (1979a) in the infinite outer-scale limit, but a means for dealing with the effect of a finite outer scale on phase scintillation has been incorporated in WBMOD. Similarly, a means has been provided for accommodating multiple-scatter effects on intensity scintillation that should suffice for practical applications.

The descriptive irregularity model is based on numerous observations (Fremouw and Bates, 1971; Fremouw and Rino, 1978), but most particularly on observations of phase scintillation performed in the DNA Wideband Satellite Experiment (Fremouw et al, 1978). The most significant caveat about use of WBMOD, however, is that it has been calibrated quantitatively against Wideband data from only a single station in the northern auroral zone (Poker Flat, Alaska). As described in Section III, the descriptive model was developed by iterative comparison with most of the Wideband data population from Poker Flat, with a portion of the population reserved for final comparative tests.

In Figure 10, we present model comparisons with two data sets not used in iterative development. The data shown are from the west-intermediate nighttime (left) and daytime (right) corridors, collected under moderately disturbed geomagnetic conditions ($3- \leq K_p \leq 5+$). The model was run for the geometry and time of a representative pass in each corridor, using a K_p of 4 and a sunspot number of 50 (approximately the weighted-mean value for the Wideband experiment, as described in Section III C). The figure corroborates that the model describes the general level and the main features of auroral-zone phase scintillation with rather satisfactory fidelity (within a factor of two, say, for multi-pass data sets).

As in Figures 7 and 8, there is some tendency for the model to underestimate nighttime scintillation severity, especially at the lowest subauroral latitudes, and to overestimate daytime auroral-zone scintillation. Investigation of scintillation conditions at the plasmopause and in the subauroral ionospheric trough should remedy the former deficiency, which could be of operational significance under very disturbed conditions (Figure 9). The latter may be more difficult to deal with and the shape of the daytime calculated curve in

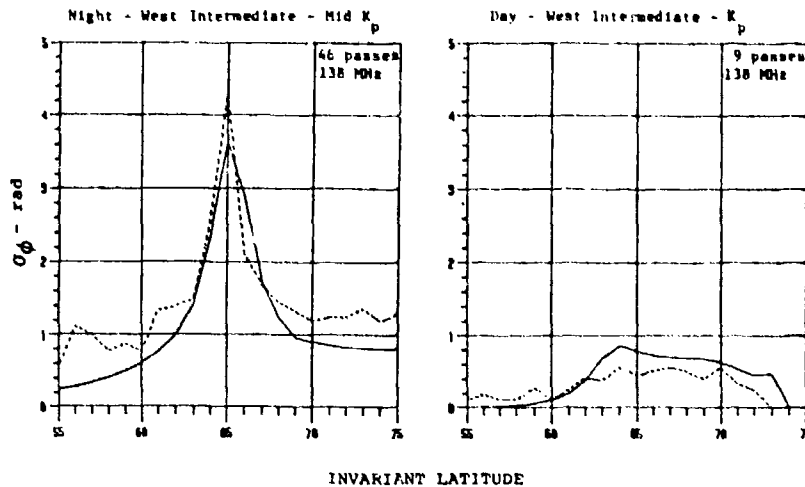


Figure 10. Comparison of model results (solid) with observed values (broken) of VHF phase scintillation index from two dissimilar data sets not used in iterative development of the model.

Figure 10 is consistent with the suggestion based on its counterpart in Figure 9 that the field-aligned axial ratio in the dayside auroral ionosphere is smaller than that included in the present model.

In closing, we re-emphasize that users of the code should judiciously select options according to their specific needs and according to the various model limitations described in this report. The model ought to be most reliable for describing auroral-zone scintillation, especially in the Alaskan sector. It has been far less reliably compared with observations of equatorial scintillation. Moreover, it is much more reliable for phase-scintillation calculations in low-orbiting applications than in geostationary applications. Users desiring phase information in the latter situation should consider providing their own estimates of ionospheric drift velocity, although the code will provide default values if desired. Finally, the model has been checked much more thoroughly against phase data than against measurements of intensity scintillation.

A new contractual effort is being undertaken to extend and improve the irregularity model in WBMOD. Emphasis is continuing to be put on phase scintillation at auroral latitudes, but the effort extends beyond that particular topic. First priority is on describing longitudinal differences in high-latitude scintillation and related seasonal effects (Basu, 1975). A concerted attempt also will be made to extend WBMOD's irregularity description to the polar caps and the plasmopause. In conjunction with extension of the model, its results will be compared with intensity scintillation data as well as with phase data.

REFERENCES

- Aarons, J., J. P. Mullen, and H. E. Whitney (1969), "The Scintillation Boundary," J. Geophys. Res. **74** (3), 884-889.
- Basu, Sunanda (1975), "Universal Time Seasonal Variations of Auroral Zone Magnetic Activity and VHF Scintillation," J. Geophys. Res., **80** (34), 4725-4728.
- Basu, S. and S. Basu (1981), "Modelling of Phase and Amplitude Scintillations at High Latitudes with AE-D Irregularity Data," paper presented at National Radio Science Meeting (Winter URSI), Boulder, CO.
- Booker, H. G., and J. A. Ratcliffe, and D. H. Shinn (1950), "Diffraction from an Irregular Screen with Applications to Ionospheric Problems," Phil. Trans. Roy. Soc. Ser. A., **242**, 579.
- Driggs, B. H., and I. A. Parkin (1963), "On the Variation of Radio Star and Satellite Scintillations with Zenith Angle," J. Atmos. Terr. Phys., **25** (6), 339-366.
- Cronyn, W. M. (1970), "The Analysis of Radio Scattering and Space-Probe Observations of Small-Scale Structure in the Interplanetary Medium," Astrophys. J., **161**, 755-762.
- Fremouw, E. J. (1981a) "Geometrical Control of the Ratio of Intensity and Phase Scintillation Indices," J. Atmos. and Terr. Phys., **42**, 775-782.
- Fremouw, E. J. (1980b), "Proposal for Improvement and Extension of the Scintillation Model in Program WBMOD," PD-NW-80-231P, Physical Dynamics, Inc., Bellevue, WA.
- Fremouw, E. J., D. J. Barnes, R. C. Livingston, M. D. Cousins, B. C. Fair, G. K. Durfey (1974), "Wideband Satellite Experiment -- Preparations for Launch," Final Report-Phase III. SRI Project 1972, Stanford Research Institute, Menlo Park, CA.
- Fremouw, E. J. and H. F. Bates (1971), "Worldwide Behavior of Average VHF-UHF Scintillation," Rad. Sci., **6**, 863-869.
- Fremouw, E. J. and J. M. Lansinger (1979), "Continued Geophysical Analysis of Coherent Satellite Scintillation Data," PD-NW-79-213R, Annual Report, Contract F49620-78-C-0014, Physical Dynamics Inc., Bellevue, WA.
- Fremouw, E. J. and J. M. Lansinger (1980), "Computer Modeling of Auroral-Zone Ionospheric Scintillation," Eimonthly Progress Report No. 3, Contract No. DNA001-79-C-0372, Project No. PD-NW-79-179, Physical Dynamics Inc., Bellevue, WA.
- Fremouw, E. J., J. M. Lansinger, and D. A. Miller (1980), "Further Geophysical Analysis of Coherent Satellite Scintillation Data," PD-NW-81-237R, Annual Report, Contract F59620-78-C-0014, Physical Dynamics, Inc., Bellevue, WA.
- Fremouw, E. J., R. L. Leadabrand, R. C. Livingston, M. D. Cousins, C. L. Rino, B. C. Fair, and R. A. Long (1976), "Early Results from the DNA Wideband Satellite Experiment -- Complex-Signal Scintillation," Rad. Sci., **13** (1), 167-187.
- Fremouw, E. J., R. C. Livingston, and D. A. Miller (1980), "On the Statistics of Scintillating Signals," J. Atmos. Terr. Phys., **42**, 717-731.
- Fremouw, E. J., and D. A. Miller, (1978), "Statistical Behavior of Signals from the Wideband Satellite," DNA Report 4818, Contract DNA001-78-C-0042, Physical Dynamics Inc., Bellevue, WA.

- Fremouw, E. J. and C. L. Rino (1973), "An Empirical Model for Average F-Layer Scintillation at VHF/UHF," Radio Science, 8, March, 213-222.
- Fremouw, E. J. and C. L. Rino (1976), "Modeling of Transionospheric Radio Propagation," RADC-TR-76-35, Rome Air Development Center, Griffiss AFB, NY.
- Fremouw, E. J. and C. L. Rino (1978), "A Signal-Statistical and Morphological Model of Ionospheric Scintillation," Proc. of AGARD Conference on Operational Modeling of the Aerospace Propagation Environment, Ottawa, Canada.
- Fremouw, E. J., C. L. Rino, A. R. Hessing, and V. E. Hatfield (1977a), "A Transionospheric Communication Channel Model," Quarterly Technical Report 7, Contract F30602-75-C-0236, Stanford Research Institute, Menlo Park, CA.
- Fremouw, E. J., C. L. Rino, R. C. Livingston, and M. C. Cousins (1977b), "A Persistent Subauroral Scintillation Enhancement Observed in Alaska," Geophys. Res. Ltrs., 4 (11), 539.
- Koster, J. R., I. Katsriku, and M. Tete (1966), "Studies of the Equatorial Ionosphere Using Transmission from Active Satellites," Annual Summary Report 1, Contract AF61(052)-800, University of Ghana-Legon, Accra, Ghana.
- Livingston, R. C., C. L. Rino, J. P. McClure, and W. B. Hanson (1981), "Spectral Characteristics of Medium-Scale Equatorial F-Region Irregularities," paper submitted to J. Geophys. Res.
- Martin, E. and J. Aarons (1977), "F Layer Scintillations and the Aurora," J. Geophys. Res., 82, 2717-2722.
- Moorcroft, D. R. and K. S. Arima (1972), "The Shape of the F-Region Irregularities Which Produce Satellite Scintillations -- Evidence for Axial Asymmetry," J. Atmos. Res., 34, 437-450.
- Rino, C. L. (1979a), "A Power Law Phase Screen Model for Ionospheric Scintillation. 1. Weak Scatter," Rad. Sci., 14 (6), 1135.
- Rino, C. L. (1979b), "A Power Law Phase Screen Model for Ionospheric Scintillation. 2. Strong Scatter," Rad. Sci., 14 (6), 1147.
- Rino, C. L. and E. J. Fremouw (1977), "The Angle Dependence of Singly Scattered Wavefields," J. Atmos. and Terr. Phys., 39, 859.
- Rino, C. L., E. J. Fremouw, A. R. Hessing, and V. E. Hatfield (1978), "Two Fortran Programs for Calculating Global Ionospheric Amplitude and Phase Scintillation," RADC-TR-78-87, Rome Air Development Center, Griffiss AFB, NY.
- Rino, C. L., E. J. Fremouw, R. C. Livingston, M. D. Cousins, and B. C. Fair (1977), "Wideband Satellite Observations," DNA Report 4399F, Contract No. DNA001-75-C-0111, SRI Project 3795, SRI International, Menlo Park, CA.
- Rino, C. L., R. C. Livingston, and S. J. Matthews (1978), "Evidence for Sheetlike Auroral Ionospheric Irregularities," Geophys. Res. Ltrs., 5 (12), 1039.
- Rino, C. L. and S. J. Matthews (1978), "On the Interpretation of Ionospheric Scintillation Data Using a Power-Law Phase Screen Model -- Weak Scatter," Tech. Report 2, SRI Project 6434, Contract DNA001-77-C-0220, SRI International, Menlo Park, CA.
- Rumsey, V. H. (1975), "Scintillations Due to a Concentrated Layer With a Power-Law Turbulence Spectrum," Rad. Sci., 10 (1), 107-114.

Scott, R. C. and D. L. Knepp (1978), "Comparison of Signal Scintillation Models," DNA 4652T, Topical Report for Period February 1978 - June 1978, Contract DNA001-77-C-0096, Mission Research Corp., Santa Barbara, CA.

Singleton, D. C. (1970), "Dependence of Satellite Scintillations on Zenith Angle and Azimuth," J. Atmos. Terr. Phys., 32, 789-803.

Singleton, D. G. (1973), "The Dependence of High-Latitude Ionospheric Scintillations on Zenith Angle and Azimuth," J. Atmos. Terr. Phys., 35, 2253-2265.

Trembka, B. T. and J. C. Cain (1974), "Computation of the IGRF: I. Spherical Expansions," X-992-74-303, Goddard Space Flight Center (NASA), Greenbelt, MD.

DISTRIBUTION LIST

DEPARTMENT OF DEFENSE

Assistant Secretary of Defense
Comm, Cmd, Cont & Intell
ATTN: Dir of Intelligence Sys, J. Babcock

Command & Control Technical Center
ATTN: C-650, G. Jones

Defense Nuclear Agency
ATTN: NAFD
ATTN: STNA
ATTN: RAEE
ATTN: NATD
3 cy ATTN: RAAE
4 cy ATTN: TITL

Defense Technical Information Center
12 cy ATTN: DD

Field Command
Defense Nuclear Agency
ATTN: FCPR

Field Command
Defense Nuclear Agency
Livermore Branch
ATTN: FCPRL

Interservice Nuclear Weapons School
ATTN: TTV

WWMCCS System Engineering Org
ATTN: R. Crawford

DEPARTMENT OF THE ARMY

Atmospheric Sciences Laboratory
U.S. Army Electronics R&D Command
ATTN: DELAS-EO, F. Niles

U.S. Army Chemical School
ATTN: ATZN-CM-CS

U.S. Army Communications Command
ATTN: CC-OPS-W
ATTN: CC-OPS-WR, H. Wilson

U.S. Army Nuclear & Chemical Agency
ATTN: Library

U.S. Army Satellite Comm Agency
ATTN: Document Control

DEPARTMENT OF THE NAVY

COMSPTEVFOR
Department of the Navy
ATTN: Code 605, R. Berg

Naval Ocean Systems Center
ATTN: Code 532, J. Bickel
ATTN: Code 5322, M. Paulson
3 cy ATTN: Code 5324, W. Moler
3 cy ATTN: Code 5323, J. Ferguson

DEPARTMENT OF THE NAVY (Continued)

Naval Research Laboratory
ATTN: Code 4780, S. Ossakow
ATTN: Code 7950, J. Goodman

Naval Space Surveillance System
ATTN: J. Burton

Naval Telecommunications Command
ATTN: Code 341

Office of Naval Research
ATTN: Code 465
ATTN: Code 420
ATTN: Code 421

DEPARTMENT OF THE AIR FORCE

Aerospace Defense Command
Department of the Air Force
ATTN: DC, T. Long

Air Force Geophysics Laboratory
ATTN: OPR, H. Gardiner
ATTN: OPR-1
ATTN: OPR, A. Stair
ATTN: S. Basu
ATTN: PHP
ATTN: PHI, J. Buchau
ATTN: R. Thompson

Air Force Weapons Laboratory
Air Force Systems Command
ATTN: SUL
ATTN: NTYC
ATTN: NTN

Air Force Wright Aeronautical Lab
ATTN: W. Hunt
ATTN: A. Johnson

Air Logistics Command
Department of the Air Force
ATTN: OO-ALC/MM, R. Blackburn

Air University Library
Department of the Air Force
ATTN: AUL-LSE

Air Weather Service, MAC
Department of the Air Force
ATTN: DNXF, R. Babcock

Assistant Chief of Staff
Studies & Analyses
Department of the Air Force
ATTN: AF/SASC, W. Keaus
ATTN: AF/SASC, C. Rightmeyer

Electronic Systems Division
Air Force Systems Command
ATTN: DCKC, J. Clark

DEPARTMENT OF THE AIR FORCE (Continued)

Foreign Technology Division
Air Force Systems Command
ATTN: TQTD, B. Ballard
ATTN: NIIS, Library

Headquarters Space Division
Air Force Systems Command
ATTN: SKY, C. Kennedy
ATTN: SKA, D. Bolin

Headquarters Space Division
Air Force Systems Command
ATTN: YZJ, W. Mercer

Headquarters Space Division
Air Force Systems Command
ATTN: E. Butt

OTHER GOVERNMENT AGENCY

Institute for Telecommunications Sciences
National Telecommunications & Infor Admin
ATTN: W. Utlacut
ATTN: A. Jean
ATTN: L. Berry

DEPARTMENT OF ENERGY CONTRACTORS

EG&G, Inc
ATTN: D. Wright
ATTN: J. Colvin

Lawrence Livermore National Lab
ATTN: Technical Info Dept, Library

Los Alamos National Lab
ATTN: D. Simons

Sandia National Lab
ATTN: Org 1250, W. Brown

DEPARTMENT OF DEFENSE CONTRACTORS

Aerospace Corp
ATTN: I. Garfunkel
ATTN: S. Bower
ATTN: D. Olsen
ATTN: N. Stockwell
ATTN: R. Slaughter
ATTN: V. Josephson
ATTN: T. Salmi
ATTN: J. Straus

University of Alaska
ATTN: T. Davis
ATTN: N. Brown
ATTN: Technical Library

BDM Corp
ATTN: L. Jacobs
ATTN: T. Neighbors

Berkeley Research Associates, Inc
ATTN: J. Workman

Communications Satellite Corp
ATTN: D. Fang

DEPARTMENT OF DEFENSE CONTRACTORS (Continued)

Cornell University
ATTN: M. Kelly
ATTN: D. Farley, Jr

ESL, Inc
ATTN: J. Marshall

General Research Corp
ATTN: J. Ise, Jr
ATTN: J. Garbarino

Harris Corp
ATTN: E. Knick

University of Illinois
ATTN: Sec Supervisor for K. Yeh

Institute for Defense Analyses
ATTN: E. Bauer

JAYCOR
ATTN: J. Sperling

Kaman Tempo
ATTN: DASIAC
ATTN: W. McNamara
ATTN: T. Stephens
ATTN: W. Knapp

Linkabit Corp
ATTN: I. Jacobs

M.I.T. Lincoln Lab
ATTN: D. Towle

Mission Research Corp
ATTN: R. Kilb
ATTN: R. Bogusch
ATTN: Tech Library
ATTN: R. Hendrick
ATTN: D. Sappenfield
ATTN: S. Gutsche
ATTN: F. Fajen

Mitre Corp
ATTN: G. Harding
ATTN: A. Kymmel
ATTN: B. Adams
ATTN: C. Callahan

Mitre Corp
ATTN: M. Horrocks
ATTN: J. Wheeler
ATTN: W. Foster
ATTN: W. Hall

Pacific-Sierra Research Corp
ATTN: H. Brode

Pennsylvania State University
ATTN: Ionospheric Research Lab

Physical Dynamics, Inc
4 cy ATTN: E. Fremouw
4 cy ATTN: J. Lansinger

DEPARTMENT OF DEFENSE CONTRACTORS (Continued)

Physical Research, Inc
ATTN: R. Deliberis

R & D Associates
ATTN: R. Lelevier
ATTN: M. Gantsweg
ATTN: B. Gabbard
ATTN: P. Haas

Rand Corp
ATTN: C. Crain
ATTN: E. Bedrozian

Science Applications, Inc
ATTN: L. Linson

Sylvania Systems Group
ATTN: M. Cross

DEPARTMENT OF DEFENSE CONTRACTORS (Continued)

SRI International
ATTN: R. Leadabrand
ATTN: C. Rino
ATTN: W. Chesnut
ATTN: R. Livingston
ATTN: R. Tsunoda
ATTN: M. Baron
ATTN: A. Burns

Tri-Com, Inc
ATTN: D. Murray

Utah State University
ATTN: K. Baker
ATTN: L. Jensen
ATTN: J. Dupnik